Enteric glia regulate Paneth cell secretion and intestinal microbial ecology

Aleksandra Prochera[1], Anoohya N. Muppirala[1], Gavin A. Kuziel[1,2,7,#], Salima Soualhi[1,#], Amy Shepherd[1,#], Liang Sun[3], Biju Issac[3], Harry J. Rosenberg[1,4], Farah Karim[5], Kristina Perez[1], Kyle H. Smith[6], Tonora H. Archibald[4], Seth Rakoff-Nahoum[1,2,7], Susan J. Hagen[6], Meenakshi Rao[1*]

1. Division of Gastroenterology, Department of Pediatrics, Boston Children's Hospital and Harvard Medical School, 300 Longwood Ave, Boston, MA 02115, USA
2. Division of Infectious Diseases, Department of Pediatrics, Boston Children's Hospital and Harvard Medical School, 300 Longwood Ave, Boston, MA 02115, USA
3. Research Computing, Department of Information Technology, Boston Children's Hospital, 300 Longwood Ave, Boston, MA 02115, USA
4. Department of Pathology, Beth Israel Deaconess Medical Center, Boston, MA, USA
5. Institute of Human Nutrition, Columbia University Irving Medical Center, New York, NY, USA
6. Department of Surgery, Beth Israel Deaconess Medical Center, Boston, MA, USA
7. Department of Microbiology, Harvard Medical School, Boston, MA 02115, USA

# denotes equal contribution
* corresponding author

Correspondence: Meenakshi Rao, MD, PhD, Boston Children's Hospital, 300 Longwood Ave, Division of Gastroenterology, Enders 659, Boston, MA 02115

Abstract

Glial cells of the enteric nervous system (ENS) interact closely with the intestinal epithelium and secrete signals that influence epithelial cell proliferation and barrier formation *in vitro*. Whether these interactions are important *in vivo,* however, is unclear because previous studies reached conflicting conclusions [1]. To better define the roles of enteric glia in steady state regulation of the intestinal epithelium, we characterized the glia in closest proximity to epithelial cells and found that the majority express *PLP1* in both mice and humans. To test their functions using an unbiased approach, we genetically depleted PLP1$^+$ cells in mice and transcriptionally profiled the small and large intestines. Surprisingly, glial loss had minimal effects on transcriptional programs and the few identified changes varied along the gastrointestinal tract. In the ileum, where enteric glia had been considered most essential for epithelial integrity, glial depletion did not drastically alter epithelial gene expression but caused a modest enrichment in signatures of Paneth cells, a secretory cell type important for innate immunity. In the absence of PLP1$^+$ glia, Paneth cell number was intact, but a subset appeared abnormal with irregular and heterogenous cytoplasmic granules, suggesting a secretory deficit. Consistent with this possibility, ileal explants from glial-depleted mice secreted less functional lysozyme than controls with corresponding effects on fecal microbial composition. Collectively, these data suggest that enteric glia do not exert broad effects on the intestinal epithelium but have an essential role in regulating Paneth cell function and gut microbial ecology.

Introduction

The intestinal epithelium is an important interface between an animal and its external environment, not just as a physical barrier but also as a dynamic regulator of digestion, energy balance, and mucosal immunity. The ENS, the intrinsic nervous system of the digestive tract, directs many intestinal epithelial functions. Glia are major cellular components of the ENS distributed throughout the radial axis of the intestine, from the muscular outer walls to the inner mucosal layer containing the epithelium. Most studies of enteric glia have focused on the cells which closely associate with neuronal soma in the myenteric plexus and have uncovered numerous roles for these glia in the regulation of neuronal functions in both health and disease [2], [3]. Many enteric glia, however, are located outside the myenteric plexus in the mucosa where they closely appose intestinal epithelial cells [4]–[8], raising the possibility that mucosal glia directly regulate epithelial cell functions.

Several enteric glia-derived cues, ranging from small molecules to growth factors, can alter epithelial cell proliferation and cell-cell adhesion *in vitro* (reviewed in [1]), supporting the possibility of glial-epithelial interactions. In the intestine, however, none of these factors are made exclusively by glia [1]. Moreover, studies in which enteric glia were depleted or disrupted *in vivo* have reported conflicting findings in terms of epithelial effects. For example, chemical gliotoxins do not cause major epithelial deficits [9], [10]. In contrast, a chemical-genetic model using a human *GFAP* promoter fragment to target glia in mice showed profound epithelial barrier defects and fulminant inflammation specifically in the distal small intestine [11]. Subsequent studies by multiple groups using more targeted systems to deplete or functionally disrupt glia defined by *Plp1*, *Sox10,* or *Gfap* expression, however, have not supported this finding. They found no major defects in epithelial properties or increased vulnerability to inflammation upon glial disruption even though all of these models exhibited deficits in other ENS-regulated functions, such as motility [12]–[15]. One study reported that simultaneous depletion of *Plp1*- and *Gfap*-expressing populations could provoke intestinal inflammation, implicating a subset of glia with particularly high *Gfap* transcript expression in the regulation of epithelial turnover through the secretion of Wnt proteins [15]. Genetic disruption of Wnt secretion in *Gfap*$^{+}$ cells, however, affected epithelial turnover only upon radiation injury [15]. Thus, it largely remains unclear what, if any, epithelial functions are enteric glia necessary for *in vivo* at steady state.

To better delineate the functional significance of enteric glial-epithelial interactions in homeostasis, first we characterized the molecular phenotype of mucosal glia along the crypt-villus axis in both mice and humans. We found that *Plp1* was the most widely expressed marker of mucosal glia in both species, supporting the use of its promoter to probe glial functions *in vivo*. Then, to interrogate glial functions in an unbiased way, we depleted *Plp1*$^{+}$ cells in mice and examined gene expression along the longitudinal axis of the intestine. Surprisingly, glial loss had minimal effects on the intestinal transcriptome or the cellular composition of the epithelium. Targeting *Plp1*$^{+}$ cells, however, caused a specific defect in Paneth cells leading to enriched gene expression signatures, diminished antimicrobial peptide secretion, and altered gut microbial composition. These observations uncover a novel link between enteric glia and Paneth cells and establish a role for enteric glia in regulating epithelial function in the healthy intestine *in vivo*.

Results

Plp1 expression broadly marks glia in the gut mucosa

Enteric glia, like Schwann cells in the periphery, are neural crest-derived and have been identified within tissues by molecular markers including *Sox10, Gfap, Plp1,* and *S100b*. Although most glia within enteric ganglia are labeled by these markers, heterogeneity in their expression has been reported [16], [17], particularly in glia located outside the myenteric plexus [18]. To determine which marker is most broadly expressed by mucosal glia and would thus be most useful for genetic interrogation of glial-epithelial interactions, we analyzed publicly available single-cell RNA sequencing (scRNAseq) datasets of human and mouse intestinal mucosa.

In the non-diseased human small and large intestines, expression of *SOX10* and *PLP1* was restricted to cluster of cells with a glial signature (Fig. 1A, Supp. Fig. 1A). *S100B* was highly expressed by cells in this cluster but also detected in non-glial cells including macrophages and monocytes; *GFAP* was overall undetectable (Fig. 1A, Supp. Fig. 1A). To validate these findings, we examined expression of the corresponding proteins by immunohistochemistry (IHC) in the human small intestine and found SOX10-, PLP1-, and S100B-immunoreactive cells in three compartments along the radial axis: the mucosa, enteric ganglia in the submucosal and myenteric plexuses, as well as intramuscular glia in the muscularis externa (Supp. Fig. 2A-B, D). GFAP-immunoreactive cells were readily found within enteric ganglia but were rare in the mucosa (Supp. Fig. 2C). These observations are consistent with a recent study that examined SOX10, GFAP, and S100B by IHC in the human colon and found little to no GFAP, but robust SOX10 and S100B expression across all three compartments [19]. In the small intestine of patients with inflammatory bowel disease (IBD), *SOX10*, *PLP1,* and *S100B* transcripts were highly enriched in mucosal glia while *GFAP* was enriched in various non-glial cells including fibroblasts and immune cells (Fig. 1B). In sum, *SOX10, PLP1 and S100B* are broadly expressed by human enteric glia across the radial axis of the gut, including mucosal glia, in both healthy and inflamed states, with *SOX10* and *PLP1* exhibiting the most cell type specificity.

In mice, we previously showed that PLP1 is widely expressed by enteric glia across the radial axis of the small and large intestines where its expression largely overlaps with S100B; a more limited subset expresses GFAP [18]. Consistent with these observations, analysis of scRNAseq data from the mouse colonic mucosa showed that *Plp1* is broadly expressed across the single putative cluster of mucosal glia; *Gfap*, *S100b,* and *Sox10* are also detectable in this cluster to variable extents (Supp. Fig. 1B). Given recent observations that a subset of $Gfap^{high}/Plp1^{low}$ mucosal glia might be particularly important for epithelial regulation in the mouse small intestine [15], we closely compared *Plp1* and *Gfap* expression in the mouse ileum. We performed whole-mount IHC for GFAP in Plp1-eGFP reporter mice to ensure the detection of colocalization despite any potential differences in subcellular distribution. Previous work from our lab and others has validated that eGFP expression in this reporter strain faithfully mirrors endogenous PLP1 expression within the enteric and central nervous systems [18], [20]. In adult Plp1-eGFP mice, we found that mucosal glia diverged sharply in terms of marker expression based on their location along the crypt-villus axis. While the majority of villus $Plp1^{+}$ cells co-expressed GFAP, virtually none of the crypt-associated $Plp1^{+}$ cells did so (Fig. 1C-D). With rare exceptions in some villi, GFAP-immunoreactive cells that did not express *Plp1* were largely undetectable. Together, these observations indicate that *Plp1* expression broadly marks enteric glia in mouse and human tissues and is among the most sensitive and specific markers for glia in the gut mucosa.

Genetic depletion of enteric glia causes muted and region-specific changes in the intestinal transcriptome

To determine what aspects of intestinal homeostasis enteric glia are essential for *in vivo*, we took an unbiased approach. We examined changes in gene expression that occur upon glial loss in three different intestinal regions: proximal small intestine (duodenum), distal small intestine (ileum), and the large intestine (colon). We depleted the cells by administration of tamoxifen to young adult Plp1^{CreER} Rosa26$^{DTA/+}$ mice, which we previously showed exhibit loss of the majority of S100B- and SOX10-expressing enteric glia, including 90% of mucosal glia [12]. In this model, glia are lost within 5 days of tamoxifen induction (5dpt) and remain stably depleted through 14dpt; notably female, but not male, mice have intestinal dysmotility [12]. To facilitate detection of direct effects of glia rather than indirect effects related to dysmotility, we isolated intestinal segments from male Plp1^{CreER} Rosa26$^{DTA/+}$ mice and Cre-negative Rosa26$^{DTA/+}$ littermate controls at 11dpt and performed bulk RNA-sequencing (Fig. 2A). Surprisingly, there were minimal changes observed in the transcriptome in all 3 regions of the intestine though the mice exhibited robust depletion of S100B$^+$ glia by IHC. In the duodenum and ileum, differential gene expression analysis by DESeq2 revealed no genes that reached the standard threshold for statistical significance of p_{adj}<0.05 (Fig. 2B, Supp. Fig. 3). In the colon, only five genes were differentially expressed, most of which were upregulated in glial-ablated mice (Fig. 2B, Supp. Fig. 3). These results suggest that acute depletion of enteric glia in male mice has limited effects on the intestinal transcriptome.

Enteric glia represent a relatively small proportion of cells in the intestine. Reasoning that transcriptional changes resulting from the biological effects of enteric glial loss might be muted in magnitude but consistent along the length of the intestine, we identified genes differentially expressed in Cre$^-$ (controls) compared to Cre$^+$ (glial-ablated) mice using a more lenient significance threshold of p<0.05 and then performed DiVenn analysis [25] to identify changes that were shared across the duodenum, ileum, and colon. Most genes that were differentially expressed were highly specific to one region of the intestine (Fig. 2C). While 331, 516, and 916 genes were changed uniquely in duodenum, ileum, and colon, respectively, only 16 to 29 genes were shared between pairs of tissues (Fig. 2C). Remarkably, only two genes were differentially expressed between Cre$^-$ and Cre$^+$ mice in all three tissue regions (*Igkv4-91* and *Ighv1-58*), suggesting that enteric glia exert region-specific effects along the longitudinal axis of the intestine.

Focusing on the colon, which showed the most evidence of altered gene expression upon glial loss, we examined the expression of *Lyz1*, the top gene upregulated in Cre$^+$ mice (Fig. 2B, Supp Fig. 3B). LYZ1 is an antimicrobial peptide (AMP) that is highly and relatively specifically expressed by Paneth cells in the small intestine (Supp. Fig. 4A) [26]. Quantitative RT-PCR (qPCR) of colonic tissue isolated from independent cohorts of Plp1^{CreER} Rosa26$^{DTA/+}$ mice confirmed upregulation of *Lyz1* in the colons of Cre$^+$ mice (Supp. Fig. 4B). Reactome pathway analysis of differentially enriched genes in the colon also highlighted pathways characteristic of Paneth cells including defensins and other AMPs. Paneth cells are not typically present in the healthy mouse colon and their ectopic appearance is considered a marker of inflammation [27]–[30]. To determine if glial depletion provoked the formation of ectopic Paneth cells, we performed IHC for LYZ1 and DEFA5, a second and independent marker of Paneth cells [31], [32]. Although both markers robustly labeled Paneth cells in the small intestine, no LYZ1- or DEFA5-immunoreactive epithelial cells were detected in the colons of either Cre$^-$ or Cre$^+$ mice (Supp. Fig. 4D). These data suggest that acute glial depletion causes transcriptional

dysregulation in the colon linked to Paneth cell biology without evidence of ectopic Paneth cells or corresponding changes in proteins.

Glia depletion selectively alters Paneth cells in the small intestine

Previous studies have indicated that glia might be most important for epithelial homeostasis in the ileum [11], [34]. Although epithelial cells are well-represented in whole gut transcriptomes, there are many other abundant cell types such as immune cells that are also present. To investigate glial effects on epithelial cells more specifically, we mechanically isolated the ileal epithelium from glial-ablated and control mice at 11dpt and examined gene expression by RNA-Seq. DESeq2 and DiVenn analysis detected minimal overlap in the transcriptional changes observed in the whole ileum compared to the ileal epithelium, supporting the utility of focused epithelial analysis (Fig. 3A).

Most intestinal epithelial cells turn over every 3-5 days [35] and thus the majority of cells represented in the epithelial transcriptome of Cre^+ mice would not have experienced glial interactions. Nevertheless, epithelial gene expression was similar in control and glial-ablated mice, mirroring the findings from whole tissue. No genes reached the $p_{adj}<0.05$ threshold of significance for differential expression (Supp. Fig. 5A-C).

The intestinal epithelium is composed of a diverse array of cells including absorptive enterocytes, $Lgr5^+$ stem cells, and various secretory cell types (Fig. 3B). To determine if glial depletion selectively affected any of these cell types, we performed gene set enrichment analysis (GSEA) using cell-type specific signatures obtained from a published scRNAseq study (Supplementary Table 1, [33]). Several of these signatures, most significantly that of Paneth cells ($p<0.001$, FDR <0.001), were enriched in the transcriptional profile of Cre^+ mice (Fig. 3B, Supp. Fig. 5D). An independent GSEA using curated cell signatures derived from bulk RNASeq studies (Supplementary Table 2) also showed an enrichment of the Paneth cell program ($p<0.001$, FDR <0.001, Supp. Fig. 5E-F).

The observed enrichment of Paneth or other secretory cell signatures could be a result of altered differentiation and/or survival. Immunostaining for molecular markers of Paneth, $Lgr5^+$, goblet, enteroendocrine, and microfold (M) cells, however, revealed no difference in their densities in Cre^+ mice compared to Cre^- littermates (Fig. 3C-D). In glial-ablated mice, all these cell types also appeared grossly normal, except for Paneth cells (Fig. 4A). Paneth cells are highly secretory cells located at the crypt base that are responsible for production and release of the bulk of small intestinal AMPs, such as LYZ1 and α-defensins, which are crucial for homeostatic regulation of the microbiome and innate immunity [26], [31], [32], [36]–[38]. Labeling Paneth cell granules with the fucose-specific lectin UEA-1, revealed that many Paneth cells in Cre^+ mice had heterogenous secretory granules, some of which appeared giant, fused, or dysmorphic (Fig. 4A). On ultrastructural analysis by transmission electron microscopy, Paneth cells in Cre^- mice had typical morphology with a pyramidal shape, extensive rough endoplasmic reticulum, and relatively homogenous, electron-dense granules with haloes, which were oriented toward the apical surface of the cell (Fig. 4B). In Cre^+ mice, Paneth cells had normal rough endoplasmic reticulum, but many exhibited a globular morphology and contained more heterogeneous granules (Fig. 4B). In contrast, neighboring intestinal stem cells in the crypt base, as well as other secretory cell types such as enteroendocrine cells and goblet cells appeared no different in Cre^- and Cre^+ mice (Supp. Fig 6). In sum, glial depletion did not provoke major shifts in small intestinal epithelial gene expression or cell composition but caused upregulation of Paneth cell genes associated with specific morphological changes that were highly specific to this cell type.

Glial depletion impairs Paneth cell secretory activity

Paneth cells secrete their granules both constitutively and in response to various stimuli, such as pathogen-associated molecular patterns [39] and cholinergic agonists [40]. At the level of individual cells, disruption of this secretory activity can manifest as accumulation and/or fusion of their secretory granules [41], [42]. The abnormal granule appearance in Cre^+ mice suggested that glial depletion might compromise Paneth cell secretion. Consistent with this possibility, the "extracellular" and "secretory" cellular compartments were most enriched in pathway analysis of Paneth cell genes that were changed in glial-depleted mice (Fig. 5A). Paneth cell secretion has often been measured in preparations of mechanically isolated epithelial crypts or enteroids [39], [43]. These preparations, however, are denervated and lack key neighboring cells including glia. To enable measurement of Paneth cell secretion in a more native environment, we developed an explant-based activity assay to measure luminal lysozyme secretion (Fig. 5B). Supporting this assay's specificity for Paneth cell-derived lysozyme, pre-treatment of mice with dithizone, a zinc chelator known to selectively deplete Paneth cell granules [44], [45], reduced detectable lysozyme activity (Fig. 5C). Utilizing this assay, we found that small intestinal explants from Cre^+ mice secreted less active lysozyme than those from Cre^- controls (Fig. 5C), indicating that glial loss disrupts Paneth cell secretion.

Cholinergic signaling regulates Paneth cell function [40], [41], [46]–[48] and genetic depletion of G proteins that act downstream of muscarinic acetylcholine receptors (AChR) alters granule morphology [49]. Muscarinic acetylcholine receptor 3 (mAChR3) is the major neurotransmitter receptor expressed by Paneth cells (Supp. Fig. 7A-B) [48]. Its expression level in the epithelium was unchanged by glial loss (log2FC = 0.104762356, p-value = 0.6474, p*adj* = 0.9999). In line with this observation, Paneth cells in Cre^+ mice remained capable of degranulation in response to the cholinergic agonist, carbachol, and secreted similar levels of lysozyme upon carbachol stimulation (Supp. Fig. 7C-D). Thus, Paneth cells in mice lacking enteric glia exhibit morphological and functional evidence of diminished secretory function at baseline but remain competent to respond to at least some stimuli.

Baseline Paneth cell secretion in Cre^+ mice could be diminished if glia are necessary for tonic Paneth cell stimulation. In the skin, another critical barrier tissue, glia are essential for the maintenance of nerve terminals, and glial depletion causes rapid and dramatic denervation [50], [51]. To determine if enteric glial depletion similarly causes intestinal epithelial denervation that might result in decreased Paneth cell stimulation, we characterized crypt-associated neuronal fibers in Cre^+ and Cre^- mice. Overall, the density of crypt innervation was no different in the two groups of mice (Supp Fig. 7E). Many types of intrinsic and extrinsic neurons innervate the intestinal epithelium. We found that most nerve fibers surrounding crypts are from cholinergic neurons and these fibers tightly associate with enteric glia (Supp. Fig. 7F-G). Given that muscarinic acetylcholine receptors are among the few neurotransmitter receptors expressed by Paneth cells (Supp. Fig. 7A-B) [48], cholinergic neurons are likely the ones most relevant to Paneth cell function. To test whether these neurons are altered by glial depletion, we assessed vesicular acetylcholine transporter (VAChT) immunoreactivity in Cre^- and Cre^+ mice. We observed no difference in the presentation of cholinergic nerve terminals that surround epithelial crypts (Supp. Fig. 7H). These observations establish that glia are not required to maintain epithelial innervation in the intestine and that Paneth cell defects in glial-depleted mice do not result from loss of cholinergic innervation.

Glial depletion alters gut microbiome composition

Paneth cell-derived antimicrobial peptides are essential for preventing microbial colonization of intestinal crypts in the small intestine [53], [54] and modulating the overall structure of the gut microbiome [37], [55]. Bacterial 16S rRNA fluorescent in situ hybridization (FISH) revealed no difference in the average distance between bacteria and intestinal crypts in Cre^- and Cre^+ mice (Supp. Fig. 8A) indicating that glial depletion does not provoke microbial invasion into crypts. To determine if enteric glial loss alters gut microbiome composition, we performed 16S ribosomal DNA sequencing of fecal pellets from Cre^- and Cre^+ mice at baseline (0dpt) and after glial loss (11dpt; Supp. Fig. 8B). Both α- and β-diversity were altered by glial depletion at 11dpt (Fig. 5D-E). β-diversity analysis, in particular, revealed clustering of samples by genotype at 11dpt ($p=0.003$), which explained a significant proportion of the inter-sample variance ($R^2 = 0.25679$, Fig. 5E).

Paneth cell secretions can influence the abundance of specific members of the gut microbiome [37], [55]. At the phylum level, use of linear discriminant analysis effect size (LEfSe) detected three phyla that were differentially abundant in Cre^+ mice at 11dpt but not 0dpt, with Firmicutes and Deferribacteres associated with glial presence and Bacteroidetes associated with glial depletion (Fig. 5F; FDR-adjusted $p<0.1$, LDA>1). At the species level, the abundance of several taxa was altered in Cre^+ mice relative to Cre^- controls at 11dpt (Fig. 5G). Many of the species associated with presence of glia were *Lactobacilli* including *Ligilactobacillus murinus* and *L. animalis,* whereas species such as *Bacteroides acidifaciens* were more associated with glial ablation. Four-way analysis of the pre- and post-induction time points confirmed these changes (Supp. Fig. 8C). *L. murinus* and *L. animalis* were previously identified among the species most depleted in the fecal microbiome of $Lyz1^{-/-}$ mice and most enriched in a Lyz1-overexpression model [55]. Taken together, these observations indicate that genetic depletion of enteric glia disrupts Paneth cell secretion of lysozyme to impact gut microbiome composition.

Discussion

Enteric glia secrete factors that influence intestinal epithelial cell properties *in vitro*, but it has remained unclear what, if any, essential roles these cells play in regulating epithelial functions *in vivo*. Here, we identify *PLP1*$^+$ cells as the glia that most closely interact with the gut epithelium and show that genetic depletion of these glia in mice does not have major effects on the intestinal transcriptome or the cellular composition of the epithelium. Enteric glial loss, however, does cause dysregulation of Paneth cell gene expression that is associated with morphological disruption of Paneth cells, diminished lysozyme secretion, and altered gut microbial composition. Together, these observations support a working model in which glia are necessary for Paneth cell secretion of proteins that modulate the composition of the gut microbiome, but unlike in the skin, are not required for maintaining epithelial innervation (Fig. 5H).

Disruption of mucosal glia provokes muted and region-specific transcriptional changes in the intestine

Comparing expression of the four molecular markers used most commonly to label enteric glia, we found that SOX10 and PLP1 were the most cell type-specific for glia in the mucosa, with little to no non-glial expression in healthy or inflamed states in both mouse and human tissues. In contrast, S100B was detectable in a subset of immune cells, while GFAP was variably expressed in the mouse mucosa and largely undetectable in human mucosal glia at the transcript and protein levels. Having identified PLP1 as the molecular marker most widely expressed by enteric glia adjacent to the epithelial layer, we utilized its promoter to probe their functional significance in adult mice using an unbiased approach. Transcriptional profiling of three different intestinal regions, quantification of cell type composition, and assessment of the

histological and ultrastructural presentation of various epithelial subtypes all indicated that genetic depletion of enteric glia does not result in broad changes to the intestinal epithelium.

Our observations are contrary to some reports of the effects of *Gfap*$^+$ cell depletion [11], [34], [56], but they are consistent with many other studies that did not uncover overt epithelial disruption when: (i) utilizing the *Plp1* or *Sox10* promoters to disrupt glia [12]–[15], (ii) targeting *Gfap*$^+$ cells in some cases [13], [14], or (iii) administering chemical gliotoxins [9], [10]. *Gfap* is often used as a marker of reactive glia in the central nervous system in the context of injury or disease. In the intestinal mucosa of humans with IBD, however, *Gfap* expression appeared most robust in non-glial cells, at least at the transcriptional level. Experimental models that employ the *Gfap* promoter to disrupt enteric glia would thus presumably also affect these non-glial cells, which may explain the dramatic epithelial phenotypes reported in some previous studies. Although glia can secrete a variety of factors that modulate epithelial proliferation and barrier integrity *in vitro*, they do not seem essential for these functions *in vivo*. This may indicate the existence of redundant mechanisms to preserve these fundamental epithelial functions *in vivo* and/or that glial-epithelial interactions are more consequential in the context of pathophysiology than normal physiology.

The GI tract exhibits functional, cellular, and molecular specializations along its longitudinal axis. The distinct transcriptional changes resulting from the ablation of PLP1$^+$ cells along this axis hint at a regional specialization of enteric glia. Consistent with this possibility, enteric glia have been shown to regulate colonic but not small intestinal GI motility [18], control secretomotor responses in the large intestine but not the upper GI tract [57], [58], and exert different immunomodulatory roles in the small and large intestines [59], [60]. The region-specific functions of enteric glia as well as the mechanisms underlying this specialization will be informative to explore.

A limitation of our study and all the others to date is the lack of enteric glial-specific molecular markers and genetic promoters. All available tools to label and manipulate enteric glia also target glia in the rest of the nervous system, making it challenging to isolate their functional significance *in vivo* and shortening experimental timeframes. Future studies utilizing viral or intersectional genetic approaches to target enteric glia more selectively may enable a better understanding of the consequences of long-term glial disruption.

Enteric glia as putative regulators of Paneth cells

Genetic depletion of enteric glia in adult mice provoked selective transcriptional, morphological, and ultrastructural disruption of Paneth cells, a highly secretory cell type of the small intestine that is important for regulation of microbial ecology and innate host defense. Although the close physical association between enteric glia and small intestinal crypts in which Paneth cells reside is well known [7], [11], [61], to our knowledge this is the first study linking enteric glia and Paneth cell biology. Loss of PLP1$^+$ enteric glia did not affect Paneth cell number, but caused many of them to lose their typical morphologies and altered the appearance of their secretory granules. These morphological changes were associated with reduced luminal secretion of lysozyme, one of the most abundant AMPs produced by Paneth cells.

Morphologic changes in Paneth cells, similar to those we observed in Cre$^+$ mice, have been reported in studies where cholinergic signaling is blocked or vagal innervation to the intestine is severed. For example, the cholinergic antagonist atropine triggers accumulation and enlargement of Paneth cell secretory granules in mice and rats [41], [62], [63]. Activation or inhibition of cholinergic signaling to Paneth cells has also been shown to increase or decrease

their secretory activity, respectively [40], [41], [46], [47]. We found that Paneth cells in glial-depleted mice remained competent to respond to cholinergic stimulation. Furthermore, unlike in the skin, glial depletion did not cause denervation. Cholinergic terminals were still present in close proximity to Paneth cells in Cre^+ mice. These observations suggest that while the infrastructure for neuroepithelial signaling remains intact in the intestines of Cre^+ mice, neurotransmission across this interface may be compromised in the absence of glia. Another potential mechanism for glial regulation of Paneth cells is through the regulation of autophagy, a process important for Paneth cell secretion [64]–[67]. We did not detect enrichment of autophagy-related pathways among the transcriptional changes in glia-deficient mice, but glial-derived signals could modulate secretory autophagy in Paneth cells indirectly. For instance, the cytokine IL-22 licenses Paneth cells for secretory autophagy in the setting of *Salmonella typhimurium* infection [68], and neurotrophic factors secreted by enteric glia are necessary for IL-22 production by group 3 innate lymphoid cells [69].

We found that genetic depletion of enteric glia was associated with altered fecal microbiome composition within days, including reduced abundance of *L. murinus* and *L. animalis* and increased abundance of several species of Bacteroidales. In mice engineered to either lack or overexpress LYZ1, the fecal abundance of both *L. murinus* and *L. animalis* together drops or increases, respectively [55]. Conversely, in ZnT2-deficient mice, which exhibit reduced lysozyme activity, *Bacteroides* is the only genus significantly increased in their feces [70]. The similarities between the shifts in microbial composition observed in these constitutive systems of Paneth cell disruption and our model of acute glial depletion support a functional link between the fecal microbial changes in Cre^+ mice and reduced LYZ1 secretion.

Overall, our results uncover a functional interaction between enteric glia and Paneth cells in the small intestine and establish a role for enteric glia in shaping gut microbial ecology. Given the strong genetic associations between Paneth cells and IBD [71], and the well-established involvement of the microbiome in a wide variety of human disorders [72], identifying the mechanisms underlying glial regulation of these secretory cells might reveal novel targets for tuning their activity for therapeutic benefit.

Acknowledgments
We are grateful to the funding sources listed below, Wendy B. Macklin (University of Colorado) for PLP-1/DM20 antibody, Andre J. Ouellette (University of California, Irvine) for the DEFA5 antibody, and members of the Rao laboratory for discussions and experimental support. We thank M. Grey and M. Rutlin for critical reading of the manuscript. The working model illustration (Fig. 5H) and schematics in Fig. 2A, Fig. 3B, Fig. 5B, and Supp. Fig. 8B were created with BioRender.com. The RNA-seq analysis was performed with the computational resources provided by the Research Computing Group at Boston Children's Hospital and Harvard Medical School (Boston, MA), including High-Performance Computing Clusters Enkefalos 2 (E2), and the BioGrids scientific software made available for data analysis.

Grant Support: This study was supported by the Schmidt Science fellowship (A.S.), NSF graduate fellowship (A.M.), Smith Family Foundation Odyssey Award (M.R.), NDSEG fellowship (G.A.K.), and NIH R01DK130836, K08DK110532, and R01DK135707 (M.R.). Core facilities utilized were supported by the Harvard Digestive Disease Center (NIH P30DK034854).

Disclosures: M.R. receives research support from Takeda Pharmaceuticals for unrelated studies.

Data Availability: The bulk RNA sequencing data from Plp1^{CreER} Rosa26$^{DTA/+}$ mice are deposited in the Gene Expression Omnibus (GEO: TBD). The bulk and single-cell RNA sequencing data sets analyzed are from previously published studies and accession numbers are listed in the Figure legends, Supplementary Tables, or Methods. All other data are available in the manuscript and the Supplementary Materials. Please contact the corresponding author for any additional information.

Author Contributions: A.P., A.N.M., S.S., A.S., G.A.K., and M.R. conceived aspects of the initial study. A.P., A.N.M., A.S., S.S., S.J.H., M.R., G.A.K., H.J.R., T.H.A., F.K., K.P., and K.H.S., and performed experiments and analyzed results. A.N.M., B.I., and L.S. performed RNA-sequencing analysis. G.A.K. performed 16S microbiome analysis. M.R. obtained funding for the studies. A.P., A.N.M., and M.R. wrote the manuscript. All authors edited and approved the final manuscript.

Materials and methods

Mice

Mice were group-housed in a specific pathogen-free facility with a 12-hour dark cycle and handled per protocols approved by the Institutional Animal Care and Use Committees of Boston Children's Hospital, adherent to the NIH Guide for the Care and Use of Laboratory Animals. Drinking water and laboratory chow were provided ad libitum. Male and female littermate mice were used for most experiments except where noted (males indicated as triangles and females as circles unless stated otherwise). PLP1^{CreER} mice (JAX 005975) and PLP1-eGFP mice (JAX 033357) were maintained on the FVB/NJ background while Rosa26$^{DTA/DTA}$ mice (JAX 009669) and ChAT-eGFP mice (JAX 007902) were maintained on C57/BL6 background. For generation of all experimental cohorts of glial-depleted mice, PLP1^{CreER} hemizygous mice were bred with Rosa26$^{DTA/DTA}$ mice to generate PLP1^{CreER} Rosa26$^{DTA/+}$ mice and Rosa26$^{DTA/+}$ littermate controls. These mice were administered 8mg of tamoxifen in corn oil once by orogastric gavage at 5-6 weeks of age, as previously described [12]. All analysis was carried out 11 days after tamoxifen administration (11dpt) unless indicated otherwise.

Immunohistochemistry

For frozen sections, tissues were first fixed in 4% paraformaldehyde (PFA)/phosphate buffered saline (PBS) for 1.5 hours (h), equilibrated in 30% sucrose/PBS and embedded, as previously described [12]. For IHC, 10-14 µm sections of intestine were incubated in blocking solution (0.1% Triton + 5% heat-inactivated goat [HINGS] or donkey serum in PBS), incubated overnight at 4°C in primary antibody/blocking solution, washed, and incubated for 1.5h at room temperature in secondary antibody or UEA-I (Vector Labs, #DL-1067-1) + DAPI. The slides were mounted in Vectashield (Vector Labs, #H-1200).

For IHC of small intestinal whole mounts, 2-3cm segments of small and large intestine from Plp1-eGFP mice were dissected, washed with ice-cold PBS, fixed in 4% PFA/PBS for 1.5 hours at 4°C, and then thoroughly washed with PBS. The samples were permeabilized with PBS, 0.5% Triton-X100, and incubated with primary antibodies in blocking buffer (5% HINGS, 20% DMSO, 0.5% PBS Triton) for 48h at room temperature (RT). They were then washed with permeabilization solution and incubated for 24h with secondary antibodies + DAPI. The whole mounts were mounted in Vectashield.

For DAB Immunochemistry, archived formalin-fixed paraffin-embedded female adult human small intestine tissue samples were used under the approved Beth Israel Deaconess Medical Center IRB protocol 2020P001104. The samples were sectioned and subjected to dewaxing with incubation at 58°C for 15-20min followed by washes in 100% xylene (2x5min). The slides were rehydrated in 100% ethanol bath (3x5min) followed by 70% ethanol incubation for 10min. Following a wash with PBS, the slides were subjected to antigen retrieval by incubation in boiling citrate buffer solution for 20min. Subsequently, a blocking solution was applied (2.5% HINGS + 2.5% BSA in 0.1% PBS-TritonX100) for 2h at RT. For PLP1 and GFAP staining, prior to staining, the sections were incubated with hydrogen peroxide blocking solution (Abcam, #ab64218) for 10min at RT. Primary antibodies in the blocking solution were applied for overnight incubation at 4°C. VECTASTAIN Elite ABC-HRP Kit PK-(Vector Labs, #6100) and ImmPACT DAB Substrate Kit, Peroxidase (Vector Labs, #SK-4105) were used according to the manufacturer's instructions. Briefly, the slides were washed, incubated with biotinylated goat anti-rabbit IgG secondary antibody (1:500 in the blocking solution) for 2h at RT, washed, and subjected to VECTASTAIN ABC solution (prepared 30min in advance) for 45 minutes at RT. Subsequently, they were washed and incubated with the DAB solution (1:30 dilution of DAB

reagent in ImmPACT DAB diluent) until a visible change to brown color was observed (20s-2min). The slides were washed and mounted in glycerol for subsequent imaging.

Target	Supplier	Catalog number	Dilution	Fluorophore	Application
CHGA	Abcam	ab-15160	1:1000	N/A	IHC
b-Catenin	R&D Systems	AF1329-SP	1:200		
DEFA5	Gift from A. Ouellette	N/A	1:1000		
E-cadherin	Life Tech	13-1900	1:400		
GFAP	Sigma-Aldrich	G9269	1:500		
LYZ1	DAKO	A0099	1:500		
MUC2	Santa Cruz Biotechnology	sc-15334	1:200		
PLP1/DM20	Gift from Wendy Macklin, Ph.D.	N/A	1:500		
S100β	DAKO	Z0311	undiluted or 1:500		
TUBB3	Biolegend	801201	1:500		
VACHT	Synaptic systems	139 103	1:500		
CD16/32 (FcR-blocking)	Biolegend	101301, clone 93	1:50	N/A	Flow cytometry
NKM 16-2-4	Miltenyi Biotec	130-102-150	1:10	PE	
CD326 (Ep-CAM)	Biolegend	118213, clone G8.8	1:50	APC	

RNA sequencing

All samples were collected between 9AM and 12PM. Mice were euthanized, and the GI tract was dissected into sterile, ice-cold PBS. The luminal content was flushed out of the tissue; fat and mesentery were trimmed. 1cm fragments of duodenum, proximal ileum, and proximal colon were cut, immersed in TRIzol reagent (Thermofisher #15596026), homogenized, frozen on dry ice, and stored at -80^{o}C until RNA extraction. For the mechanical separation of ileal epithelium, 6cm of the most distal small intestine (ileum) was used. The tissue was cut longitudinally and cleaned in ice-cold 1xPBS such that any remaining fecal/luminal content was removed. The opened ileal tissue was placed in 10ml 5mM EDTA in sterile PBS, gently mixed, and incubated on ice in a horizontal position for 10min while ensuring its complete submersion in the EDTA solution. Halfway through, the tube was gently tilted twice to mix. Subsequently, the EDTA solution was decanted, and the tissue was washed with 10ml of sterile HBSS twice. To mechanically separate the epithelial fraction, the tissues were extended epithelium-side-up on a glass slide and the epithelial layers (villi first, followed by crypts) were separated using a bent 20G needle. The epithelial content was immediately transferred to the TRIzol reagent, homogenized, frozen on dry ice, and stored at -80^{o}C until RNA extraction. RNA was extracted using phenol/chloroform extraction methods followed by a cleanup with the RNeasy Kit (Qiagen #74004). RNA samples were analyzed for purity and concentration and submitted to Novogene Corporation Inc. (Sacramento, CA, United States) for quality control, library construction, and sequencing. Sequencing was performed on Novaseq 6000 platform (20M/PE150).

RNA-seq analysis

We used trimmomatic [73] to trim the low-quality next generation sequencing (NGS) reads (-threads 20 ILLUMINACLIP:TruSeq3-PE.fa:2:30:10 LEADING:3 TRAILING:3 SLIDINGWINDOW:4:15 MINLEN:36). Subsequently, only the high-quality trimmed reads were aligned to the mouse reference genome using STAR [74]. The reads counts were calculated by featureCounts software [75]. Differentially expressed genes (DEGs) were identified by using the DESeq2 R package (adjusted p value <=0.05) [76]. For analysis of shared gene expression, DiVenn analysis was carried out as previously described [25]. GSEA analysis was performed using GSEApy [77].

Quantitative PCR

For validation of RNAseq results, two separate cohorts of PLP1-DTA mice were used. The tissues were dissected and processed as described above. RNA was extracted using phenol/chloroform extraction methods followed by a cleanup with the RNeasy Kit (Qiagen #74004). The RNA was converted to cDNA using iScript cDNA Synthesis Kit (BioRad #1708890) and the qPCR was run with SYBR Select Master Mix (Thermofisher # 4472908). The following primers were used.

Target	Forward primer	Reverse primer	Annealing temp.
Epcam	TCGCAGGTCTTCATCTTCCC	GGCTGAGATAAAGGAGATGGGT	60°C
Lyz1	ATGGCTACCGTGGTGTCAAG	CGGTCTCCACGGTTGTAGTT	58°C
Defa22	CAGCATCAGTGGCCTCAGAG	CGGCTGTGCTTGTCTCCTTTGGAG	60°C
Mmp7	CCTAGGCGGAGATGCTCACTT	GGGTACATCACAGTACCGGGA	63°C

Imaging and cell quantification

Image acquisition was carried out by investigators blinded to genotype. Animals of both sexes were analyzed. Data was analyzed using Microsoft Excel and the GraphPad Prism program (GraphPad Software, Inc.). For quantification of Alcian Blue$^+$ goblet cells, images were obtained from Cre$^+$ (n = 8) and Cre$^-$ (n = 10) animals. The number of Alcian Blue$^+$ cells per villus-crypt unit was counted and averaged per mouse. For LYZ1$^+$ Paneth cells, images of at least 50 crypts in the ileum were obtained for each Cre$^+$ (n = 4) and Cre$^-$ (n = 5) animals. The number of LYZ1$^+$ cells per crypt was counted and averaged per mouse. For Chromogranin A$^+$ EECs, images of at least 42 villi and 100 crypts in the ileum were obtained, for each Cre$^+$ (n = 3 per group) and Cre$^-$ (n = 4 per group) animal. The number of CHGA$^+$ cells per villus-crypt unit was counted and averaged per mouse. For Lgr5$^+$ cells, 6 - 9 z-stack images (20X) were obtained for each Cre$^+$ (n = 4) and Cre$^-$ (n = 4) animal. For quantification of mean fluorescence intensity (MFI), z-stacks were subjected to maximum intensity projection, and ROI's were drawn from the villus base to crypt base that defined crypt regions. MFI of the ROI was calculated and averaged per mouse. For quantification of crypt innervation, 15 random z-stack images of individual crypts were obtained for each Cre$^+$ (n = 4) and Cre$^-$ (n = 4) animal. Z-stack images were subjected to maximum intensity projection, binarization, thresholding, and smoothening. Subsequently, the signal was converted to masks, and the percentage area of TUBB3 signal coverage of the image field was calculated and averaged per mouse. A Zeiss LSM 880 confocal microscope was used to acquire images for all fluorescent IHC except for CHGA$^+$ EECs, for which a Leica DM6000B epifluorescent microscope was used.

Flow Cytometry

Flow cytometry of M cells from Peyer's Patches (PPs) was adapted from Gicheva et al., 2016 [78]. Briefly, the entire length of jejunum and ileum were dissected from Cre$^-$ and Cre$^+$ mice. 6-

Peyer's patches were harvested, placed in 1.5 mL microcentrifuge tubes with ice-cold 1xPBS, and vortexed vigorously to remove debris. After three PBS washes, the PPs were placed in 10ml of PBS with 5mM EDTA and 1mM DTT for 30 minutes at 37°C. The samples were additionally triturated to aid the dissociation. Following digestion, the cell suspension was filtered through a 40µm strainer, centrifuged at 475g for 5 minutes, and incubated with FcR-blocking antibody on ice for 10min. The cells were then stained to label M-cells (NKM 16-2-4) and epithelial cells (Ep-CAM) in FACS buffer (2% FBS +1mM EDTA) for 30 min at 4˚C. Subsequently, the cells were washed in FACS buffer and stained with DAPI (0.3ug/mL). The proportion of PE^+ APC^+ $DAPI^-$ cells out of APC^+ $DAPI^-$ cells was determined on BD LSRFortessa.

RNAscope

Intestinal tissue was dissected into ice-cold 1xPBS 1x PBS + 4mM ribonucleoside vanadyl complexes (RVC) to inhibit RNAse activity and flushed to remove fecal content. Segments of ~2cm were fixed in RNAse-free 4%PFA/PBS for 24h and incubated overnight in 30% sucrose. The tissue was embedded in pre-chilled OCT and frozen on dry ice. The tissues were stored at -80°C. For staining, 8 µm slices were sectioned and air dried at -20°C. RNAscope V2 (ACDBio #323100) was used for in situ hybridization. Briefly, the slides were washed in 1xPBS, incubated for 30min at 60°C, and post-fixed with pre-chilled 4%PFA for 15min at 4°C. Subsequently, the slides were dehydrated in increasing concentrations of RNase-free EtOH (50%, 70%, and twice 100% for 5min each), treated with hydrogen peroxide (RNAscope™ Hydrogen Peroxide Reagent) for 10min at RT, and washed in DEPC-treated water. For antigen retrieval, the slides were immersed in boiling hot RNAscope™ Target Retrieval Reagent, and incubated at 99°C for 5min. Following a wash in RT DEPC-treated water, they were incubated in 100% EtOH for 3min, dried at RT, and subjected to protease treatment (RNAscope™ Protease III Reagent) for 30 min at 40°C. After two washes with 1x PBS, probe hybridization and signal amplification were carried out according to RNAscope™ Multiplex Fluorescent V2 Assay using Lgr5-C1 probe and Opal dye 570 (Akoya Sciences). Slides were mounted with Vectashield and DAPI.

Electron microscopy

Tissues were excised, washed in PBS, cut along the mesenteric plane, pinned flat, and then fixed in 2% glutaraldehyde (Electron Microscopy Sciences, Hatfield PA) and 2.5% formaldehyde (Electron Microscopy Sciences), in 0.1M cacodylate buffer pH 7.4 containing 0.1 mM EGTA for 10 minutes at RT with gentle flushing. The tissue was then cut into small pieces, and fixed for an additional 1 hour in the same fixative at RT. Tissues were washed with 0.1 M cacodylate buffer, and then loaded into a planchette (Technotrade International, Manchester, NH) with PBS containing 20% BSA and 5% FBS, and subjected to high pressure freezing using a Wohlwend High Pressure Freezer (Technotrade International). Rapid freeze substitution, as described [79], was done using 1% osmium tetroxide, 0.5 % uranyl acetate, 95% acetone and 5% dH2O. After freeze substitution, the tissue was infiltrated with graded acetone into LX112 resin (Ted Pella, Inc. Redding ,CA). Ultrathin sections were cut with a Leica Ultracut E ultramicrotome (Leica Microsystems, Wetzlar Germany), placed on formvar and carbon coated grids, and then stained with 2% uranyl acetate (Electron Microscopy Sciences) and lead citrate (Sigma-Aldrich). Grids from each treatment were imaged using a JEOL 1400 electron microscope (JEOL USA, Peabody, MA) equipped with an Orius SC1000 digital CCD camera (Gatan, Pleasanton, CA).

Paneth cell secretion assay

All Paneth cell secretion assays were carried out from 9AM-12PM with four mice per assay except for when DTZ was administered. For DTZ experiments, the mice were administered vehicle – Li_2CO_3 solution (100mg/kg; Sigma, #255823) or DTZ in Li_2CO_3 solution (100mg/kg, Sigma, # D5130) six hours before the start of the explant experiment. Mice were euthanized and

10cm of distal small intestine was dissected into sterile, ice-cold 1xPBS. The luminal content was flushed out of the tissue, and fat and mesentery were trimmed. A 6.5-7cm fragment of the most distal small intestine was isolated and the remaining PBS was removed from the tissue. One end of the tissue was firmly tied and 150ul of sterile, ice-cold 1xPBS was pipetted into the intestinal tube. The open end of the intestine was firmly tied to create a closed cylinder filled with PBS. The length of the tissue, from one tied end to the other, was measured. The process was repeated for all samples which were kept in sterile, ice-cold 1xPBS. The explants were subsequently placed in oxygenated Krebs at 37°C and incubated continuously bubbled with Carbogen for the duration of the experiment (30min). For experiments involving carbachol, the compound was added at a concentration of 10μM at the beginning of incubation. Following incubation, one at a time, the tissues were opened up, and the luminal contents were extracted. The volume of recovered solution was measured and diluted in sterile PBS as necessary to get to a final volume of 25μL/cm of intestine. The samples were sterile-filtered with pre-wetted 0.22um syringe filters. Lysozyme activity was measured using the Lysozyme Activity Assay Kit (Abcam #ab211113) according to the manufacturer's instructions.

16S ribosomal DNA (rDNA) gene phylotyping

Male and female PLP1^{CreER} Rosa26$^{DTA/+}$ and Rosa26$^{DTA/+}$ littermate mice were group-housed segregated by sex and genotype from the time of weaning. Two to four spontaneously expelled fecal pellets were collected from each mouse at 9-10AM at two timepoints: 0dpt (prior to tamoxifen administration) and 11dpt. Fecal samples were immediately frozen and stored at -80°C. Genomic DNA for 16S rDNA amplicon next generational sequencing was isolated using the ZymoBIOMICS^{TM} – 96 DNA Kit (Zymo Research, D4309). The 16S amplicon library was prepared in a 96-well format using dual-index barcodes [80]. Libraries were cleaned with the DNA Clean and Concentrator TM – 5 Kit (Zymo Research, D4014) and then quantified by qPCR (NEBNext Library Quant Kit, NEB, E7630). 20 pM of DNA were loaded onto an Illumina MiSeq (v3, 600 cycle) and sequenced. To generate the Operational Taxonomic Unit (OTU) table for analyses of gut microbiome composition and diversity, Illumina raw reads were de-multiplexed, paired end joined, adapter trimmed, quality filtered, dereplicated, and denoised. Sequences were mapped against the publicly available 16S rDNA databases SILVA and UNITE and clustered into OTUs >= 97% nucleotide sequence identity. OTU-based microbial community diversity was estimated by calculating Shannon's alpha diversity index and Bray-Curtis beta diversity index. Differential abundance analyses were performed with LEfSe with significantly different features having an alpha value less than or equal to 0.1 and a logarithmic LDA score greater than or equal to 1.

16S bacterial rRNA FISH

16S rRNA FISH was carried out as described previously with some modifications [81]. Briefly, distal small intestine was dissected from Cre^{-} and Cre^{+} mice directly into methanol-Carnoy's fixative [60% (v/v) dry methanol, 30% (v/v) chloroform, 10% (v/v) glacial acetic acid]. Care was taken to limit exposure to aqueous solutions. The samples were kept in the fixative solution for 72h followed by washes with 100% methanol (2 x 30 min), 100% ethanol (3 x 30 minutes), xylene (2 x 20-30 min), paraffin (2 x 20-30 minutes). The samples were embedded in paraffin, sectioned, and stained as previously described [82]. Briefly, the sections were dewaxed by incubating at 60°C for 10 min, followed by two xylene baths (1 x 10min at 60°C, 1 x 10min at RT). The sections were incubated in 99.5% ethanol for 5 min, air dried, and stained with EUB338 or a control probe in a hybridization solution at 50°C overnight. Subsequently, the sections were washed and subjected to immunohistochemistry protocol as described below.

	Fluorophore	Sequence
EUB338	Cy3	GCTGCCTCCCGTAGGAGT
Nonsense control	Cy3	CGACGGAGGGCATCCTCA

Statistical Analyses

Both R 4.2.0 and Prism were used for statistical analyses and graphical visualization. For pairwise comparisons, an unpaired parametric t-test or Mann-Whitney U test was used after testing for equal variance between the groups unless stated otherwise. If variance was significantly different, unpaired parametric t-test with Welsh Correction was applied. For comparisons between more than two groups, one-way ANOVA with Tukey multiple comparisons test was used.

References

[1] A. Prochera and M. Rao, “Mini-Review: Enteric glial regulation of the gastrointestinal epithelium,” *Neurosci. Lett.*, vol. 805, p. 137215, May 2023, doi: 10.1016/j.neulet.2023.137215.

[2] L. Seguella and B. D. Gulbransen, “Enteric glial biology, intercellular signalling and roles in gastrointestinal disease,” *Nat. Rev. Gastroenterol. Hepatol.*, vol. 18, no. 8, pp. 571–587, Aug. 2021, doi: 10.1038/s41575-021-00423-7.

[3] H. J. Rosenberg and M. Rao, “Enteric glia in homeostasis and disease: From fundamental biology to human pathology,” *iScience*, vol. 24, no. 8, p. 102863, Aug. 2021, doi: 10.1016/j.isci.2021.102863.

[4] G.-L. Ferri, L. Probert, D. Cocchia, F. Michetti, P. J. Marangos, and J. M. Polak, “Evidence for the presence of S-100 protein in the glial component of the human enteric nervous system,” *Nature*, vol. 297, no. 5865, pp. 409–410, Jun. 1982, doi: 10.1038/297409a0.

[5] P. Mestres, M. Diener, and W. Rummer, “Electron Microscopy of the Mucosal Plexus of the Rat Colon,” *Cells Tissues Organs*, vol. 143, no. 4, pp. 275–282, 1992, doi: 10.1159/000147262.

[6] H.-J. Krammer and W. Kuhnel, “Topography of the enteric nervous system in Peyer’s patches of the porcine small intestine,” *Cell Tissue Res.*, vol. 272, no. 2, pp. 267–272, May 1993, doi: 10.1007/BF00302732.

[7] M. Neunlist *et al.*, “Enteric glia inhibit intestinal epithelial cell proliferation partly through a TGF-beta1-dependent pathway,” *Am. J. Physiol. Gastrointest. Liver Physiol.*, vol. 292, no. 1, pp. G231-241, Jan. 2007, doi: 10.1152/ajpgi.00276.2005.

[8] D. V. Bohórquez, L. A. Samsa, A. Roholt, S. Medicetty, R. Chandra, and R. A. Liddle, “An Enteroendocrine Cell – Enteric Glia Connection Revealed by 3D Electron Microscopy,” *PLoS ONE*, vol. 9, no. 2, p. e89881, Feb. 2014, doi: 10.1371/journal.pone.0089881.

[9] H. Aikawa and K. Suzuki, “Enteric gliopathy in niacin-deficiency induced by CNS glio-toxin,” *Brain Res.*, vol. 334, no. 2, pp. 354–356, May 1985, doi: 10.1016/0006-8993(85)90231-8.

[10] Y. Nasser *et al.*, “Role of enteric glia in intestinal physiology: effects of the gliotoxin fluorocitrate on motor and secretory function,” *Am. J. Physiol. Gastrointest. Liver Physiol.*, vol. 291, no. 5, pp. G912-927, Nov. 2006, doi: 10.1152/ajpgi.00067.2006.

[11] T. G. Bush *et al.*, “Fulminant Jejuno-Ileitis following Ablation of Enteric Glia in Adult Transgenic Mice,” *Cell*, vol. 93, no. 2, pp. 189–201, Apr. 1998, doi: 10.1016/S0092-8674(00)81571-8.

[12] M. Rao *et al.*, “Enteric Glia Regulate Gastrointestinal Motility but Are Not Required for Maintenance of the Epithelium in Mice,” *Gastroenterology*, vol. 153, no. 4, pp. 1068-1081.e7, Oct. 2017, doi: 10.1053/j.gastro.2017.07.002.

[13] R. Yuan *et al.*, “Enteric Glia Play a Critical Role in Promoting the Development of Colorectal Cancer,” *Front. Oncol.*, vol. 10, p. 595892, 2020, doi: 10.3389/fonc.2020.595892.

[14] M. L. Kovler *et al.*, “Toll-like receptor 4-mediated enteric glia loss is critical for the development of necrotizing enterocolitis,” *Sci. Transl. Med.*, vol. 13, no. 612, p. eabg3459, Sep. 2021, doi: 10.1126/scitranslmed.abg3459.

[15] M. B. Baghdadi *et al.*, “Enteric glial cell heterogeneity regulates intestinal stem cell niches,” *Cell Stem Cell*, vol. 29, no. 1, pp. 86-100.e6, Jan. 2022, doi: 10.1016/j.stem.2021.10.004.

[16] K. R. Jessen and R. Mirsky, “Astrocyte-like glia in the peripheral nervous system: an immunohistochemical study of enteric glia,” *J. Neurosci. Off. J. Soc. Neurosci.*, vol. 3, no. 11, pp. 2206–2218, Nov. 1983, doi: 10.1523/JNEUROSCI.03-11-02206.1983.

[17] W. Boesmans, R. Lasrado, P. Vanden Berghe, and V. Pachnis, “Heterogeneity and phenotypic plasticity of glial cells in the mammalian enteric nervous system,” *Glia*, vol. 63, no. 2, pp. 229–241, Feb. 2015, doi: 10.1002/glia.22746.
[18] M. Rao *et al.*, “Enteric glia express proteolipid protein 1 and are a transcriptionally unique population of glia in the mammalian nervous system,” *Glia*, vol. 63, no. 11, pp. 2040–2057, Nov. 2015, doi: 10.1002/glia.22876.
[19] N. Baidoo, G. J. Sanger, and A. Belai, “Effect of old age on the subpopulations of enteric glial cells in human descending colon,” *Glia*, vol. 71, no. 2, pp. 305–316, Feb. 2023, doi: 10.1002/glia.24272.
[20] B. S. Mallon, H. E. Shick, G. J. Kidd, and W. B. Macklin, “Proteolipid Promoter Activity Distinguishes Two Populations of NG2-Positive Cells throughout Neonatal Cortical Development,” *J. Neurosci.*, vol. 22, no. 3, pp. 876–885, Feb. 2002, doi: 10.1523/JNEUROSCI.22-03-00876.2002.
[21] H. B. Zheng *et al.*, “Concerted changes in the pediatric single-cell intestinal ecosystem before and after anti-TNF blockade,” elife, preprint, Nov. 2023. doi: 10.7554/eLife.91792.1.
[22] J. C. Martin *et al.*, “Single-Cell Analysis of Crohn’s Disease Lesions Identifies a Pathogenic Cellular Module Associated with Resistance to Anti-TNF Therapy,” *Cell*, vol. 178, no. 6, pp. 1493-1508.e20, Sep. 2019, doi: 10.1016/j.cell.2019.08.008.
[23] H.-O. Lee *et al.*, “Lineage-dependent gene expression programs influence the immune landscape of colorectal cancer,” *Nat. Genet.*, vol. 52, no. 6, pp. 594–603, Jun. 2020, doi: 10.1038/s41588-020-0636-z.
[24] M. Roulis *et al.*, “Paracrine orchestration of intestinal tumorigenesis by a mesenchymal niche,” *Nature*, vol. 580, no. 7804, pp. 524–529, Apr. 2020, doi: 10.1038/s41586-020-2166-3.
[25] L. Sun *et al.*, “DiVenn: An Interactive and Integrated Web-Based Visualization Tool for Comparing Gene Lists,” *Front. Genet.*, vol. 10, p. 421, May 2019, doi: 10.3389/fgene.2019.00421.
[26] T. Peeters and G. Vantrappen, “The Paneth cell: a source of intestinal lysozyme.,” *Gut*, vol. 16, no. 7, pp. 553–558, Jul. 1975, doi: 10.1136/gut.16.7.553.
[27] A. J. Hertzog, “The Paneth Cell,” *Am. J. Pathol.*, vol. 13, no. 3, pp. 351-360.1, May 1937.
[28] J. C. Paterson and S. H. Watson, “Paneth cell metaplasia in ulcerative colitis,” *Am. J. Pathol.*, vol. 38, no. 2, pp. 243–249, Feb. 1961.
[29] M. Tanaka *et al.*, “Spatial distribution and histogenesis of colorectal Paneth cell metaplasia in idiopathic inflammatory bowel disease,” *J. Gastroenterol. Hepatol.*, vol. 16, no. 12, pp. 1353–1359, Dec. 2001, doi: 10.1046/j.1440-1746.2001.02629.x.
[30] R. Singh, I. Balasubramanian, L. Zhang, and N. Gao, “Metaplastic Paneth Cells in Extra-Intestinal Mucosal Niche Indicate a Link to Microbiome and Inflammation,” *Front. Physiol.*, vol. 11, p. 280, Mar. 2020, doi: 10.3389/fphys.2020.00280.
[31] D. E. Jones and C. L. Bevins, “Paneth cells of the human small intestine express an antimicrobial peptide gene,” *J. Biol. Chem.*, vol. 267, no. 32, pp. 23216–23225, Nov. 1992.
[32] N. H. Salzman, D. Ghosh, K. M. Huttner, Y. Paterson, and C. L. Bevins, “Protection against enteric salmonellosis in transgenic mice expressing a human intestinal defensin,” *Nature*, vol. 422, no. 6931, pp. 522–526, Apr. 2003, doi: 10.1038/nature01520.
[33] A. L. Haber *et al.*, “A single-cell survey of the small intestinal epithelium,” *Nature*, vol. 551, no. 7680, pp. 333–339, Nov. 2017, doi: 10.1038/nature24489.
[34] A. Cornet *et al.*, “Enterocolitis induced by autoimmune targeting of enteric glial cells: A possible mechanism in Crohn’s disease?,” *Proc. Natl. Acad. Sci.*, vol. 98, no. 23, pp. 13306–13311, Nov. 2001, doi: 10.1073/pnas.231474098.
[35] A. S. Darwich, U. Aslam, D. M. Ashcroft, and A. Rostami-Hodjegan, “Meta-Analysis of the Turnover of Intestinal Epithelia in Preclinical Animal Species and Humans,” *Drug Metab. Dispos.*, vol. 42, no. 12, pp. 2016–2022, Dec. 2014, doi: 10.1124/dmd.114.058404.

[36] C. L. Wilson *et al.*, “Regulation of intestinal alpha-defensin activation by the metalloproteinase matrilysin in innate host defense,” *Science*, vol. 286, no. 5437, pp. 113–117, Oct. 1999, doi: 10.1126/science.286.5437.113.
[37] N. H. Salzman *et al.*, “Enteric defensins are essential regulators of intestinal microbial ecology,” *Nat. Immunol.*, vol. 11, no. 1, pp. 76–83, Jan. 2010, doi: 10.1038/ni.1825.
[38] H. C. Clevers and C. L. Bevins, “Paneth Cells: Maestros of the Small Intestinal Crypts,” *Annu. Rev. Physiol.*, vol. 75, no. 1, pp. 289–311, Feb. 2013, doi: 10.1146/annurev-physiol-030212-183744.
[39] T. Ayabe, D. P. Satchell, C. L. Wilson, W. C. Parks, M. E. Selsted, and A. J. Ouellette, “Secretion of microbicidal alpha-defensins by intestinal Paneth cells in response to bacteria,” *Nat. Immunol.*, vol. 1, no. 2, pp. 113–118, Aug. 2000, doi: 10.1038/77783.
[40] Y. Satoh, K. Ishikawa, Y. Oomori, M. Yamano, and K. Ono, “Effects of cholecystokinin and carbamylcholine on Paneth cell secretion in mice: a comparison with pancreatic acinar cells,” *Anat. Rec.*, vol. 225, no. 2, pp. 124–132, Oct. 1989, doi: 10.1002/ar.1092250207.
[41] Y. Satoh, “Atropine inhibits the degranulation of Paneth cells in ex-germ-free mice,” *Cell Tissue Res.*, vol. 253, no. 2, pp. 397–402, Aug. 1988, doi: 10.1007/BF00222296.
[42] A. Ahonen, “Histochemical and electron microscopic observations on the development, neural control and function of the Paneth cells of the mouse,” *Acta Physiol. Scand. Suppl.*, vol. 398, pp. 1–71, 1973.
[43] Y. Yokoi *et al.*, “Paneth cell granule dynamics on secretory responses to bacterial stimuli in enteroids,” *Sci. Rep.*, vol. 9, no. 1, p. 2710, Feb. 2019, doi: 10.1038/s41598-019-39610-7.
[44] M. Sawada, K. Takahashi, S. Sawada, and O. Midorikawa, “Selective killing of Paneth cells by intravenous administration of dithizone in rats,” *Int. J. Exp. Pathol.*, vol. 72, no. 4, pp. 407–421, Aug. 1991.
[45] S. R. Lueschow *et al.*, “Loss of murine Paneth cell function alters the immature intestinal microbiome and mimics changes seen in neonatal necrotizing enterocolitis,” *PLOS ONE*, vol. 13, no. 10, p. e0204967, Oct. 2018, doi: 10.1371/journal.pone.0204967.
[46] Y. Satoh, K. Ishikawa, Y. Oomori, S. Takeda, and K. Ono, “Bethanechol and a G-protein activator, NaF/AlCl3, induce secretory response in Paneth cells of mouse intestine,” *Cell Tissue Res.*, vol. 269, no. 2, pp. 213–220, Aug. 1992, doi: 10.1007/BF00319611.
[47] Y. Satoh, Y. Habara, K. Ono, and T. Kanno, “Carbamylcholine- and catecholamine-induced intracellular calcium dynamics of epithelial cells in mouse ileal crypts,” *Gastroenterology*, vol. 108, no. 5, pp. 1345–1356, May 1995, doi: 10.1016/0016-5085(95)90681-9.
[48] B. Dolan, A. Ermund, B. Martinez-Abad, M. E. V. Johansson, and G. C. Hansson, “Clearance of small intestinal crypts involves goblet cell mucus secretion by intracellular granule rupture and enterocyte ion transport,” *Sci. Signal.*, vol. 15, no. 752, p. eabl5848, Sep. 2022, doi: 10.1126/scisignal.abl5848.
[49] N. Watanabe *et al.*, “Requirement of Gαq/Gα11 Signaling in the Preservation of Mouse Intestinal Epithelial Homeostasis,” *Cell. Mol. Gastroenterol. Hepatol.*, vol. 2, no. 6, pp. 767-782.e6, Nov. 2016, doi: 10.1016/j.jcmgh.2016.08.001.
[50] L. Li and D. D. Ginty, “The structure and organization of lanceolate mechanosensory complexes at mouse hair follicles,” *eLife*, vol. 3, p. e01901, Feb. 2014, doi: 10.7554/eLife.01901.
[51] P. Rinwa, L. Calvo-Enrique, M.-D. Zhang, J. R. Nyengaard, P. Karlsson, and P. Ernfors, “Demise of nociceptive Schwann cells causes nerve retraction and pain hyperalgesia,” *Pain*, vol. 162, no. 6, pp. 1816–1827, Jun. 2021, doi: 10.1097/j.pain.0000000000002169.
[52] S. Yu *et al.*, “Paneth Cell Multipotency Induced by Notch Activation following Injury,” *Cell Stem Cell*, vol. 23, no. 1, pp. 46-59.e5, Jul. 2018, doi: 10.1016/j.stem.2018.05.002.
[53] U. Meyer-Hoffert *et al.*, “Secreted enteric antimicrobial activity localises to the mucus surface layer,” *Gut*, vol. 57, no. 6, pp. 764–771, Jun. 2008, doi: 10.1136/gut.2007.141481.

[54] S. Vaishnava *et al.*, "The Antibacterial Lectin RegIIIγ Promotes the Spatial Segregation of Microbiota and Host in the Intestine," *Science*, vol. 334, no. 6053, pp. 255–258, Oct. 2011, doi: 10.1126/science.1209791.
[55] S. Yu *et al.*, "Paneth Cell-Derived Lysozyme Defines the Composition of Mucolytic Microbiota and the Inflammatory Tone of the Intestine," *Immunity*, vol. 53, no. 2, pp. 398-416.e8, Aug. 2020, doi: 10.1016/j.immuni.2020.07.010.
[56] A.-C. Aube, "Changes in enteric neurone phenotype and intestinal functions in a transgenic mouse model of enteric glia disruption," *Gut*, vol. 55, no. 5, pp. 630–637, May 2006, doi: 10.1136/gut.2005.067595.
[57] V. Grubišić and B. D. Gulbransen, "Enteric glial activity regulates secretomotor function in the mouse colon but does not acutely affect gut permeability," *J. Physiol.*, vol. 595, no. 11, pp. 3409–3424, Jun. 2017, doi: 10.1113/JP273492.
[58] J.-B. Cavin, H. Cuddihey, W. K. MacNaughton, and K. A. Sharkey, "Acute regulation of intestinal ion transport and permeability in response to luminal nutrients: the role of the enteric nervous system," *Am. J. Physiol.-Gastrointest. Liver Physiol.*, vol. 318, no. 2, pp. G254–G264, Feb. 2020, doi: 10.1152/ajpgi.00186.2019.
[59] S. Ibiza *et al.*, "Glial-cell-derived neuroregulators control type 3 innate lymphoid cells and gut defence," *Nature*, vol. 535, no. 7612, pp. 440–443, Jul. 2016, doi: 10.1038/nature18644.
[60] F. Progatzky *et al.*, "Regulation of intestinal immunity and tissue repair by enteric glia," *Nature*, vol. 599, no. 7883, pp. 125–130, Nov. 2021, doi: 10.1038/s41586-021-04006-z.
[61] L. Van Landeghem *et al.*, "Enteric glia promote intestinal mucosal healing via activation of focal adhesion kinase and release of proEGF," *Am. J. Physiol. Gastrointest. Liver Physiol.*, vol. 300, no. 6, pp. G976-987, Jun. 2011, doi: 10.1152/ajpgi.00427.2010.
[62] Y. Satoh, K. Ono, and K. Moutairou, "Paneth cells of African giant rats (Cricetomys gambianus)," *Acta Anat. (Basel)*, vol. 151, no. 1, pp. 49–53, 1994.
[63] G. Sundström and H. F. Helander, "Quantitative electron microscopic studies on rat ileal Paneth cells under various physiological and experimental conditions," *Hepatogastroenterology.*, vol. 27, no. 4, pp. 286–293, Aug. 1980.
[64] K. Cadwell *et al.*, "A key role for autophagy and the autophagy gene Atg16l1 in mouse and human intestinal Paneth cells," *Nature*, vol. 456, no. 7219, pp. 259–263, Nov. 2008, doi: 10.1038/nature07416.
[65] N. Wittkopf *et al.*, "Lack of Intestinal Epithelial Atg7 Affects Paneth Cell Granule Formation but Does Not Compromise Immune Homeostasis in the Gut," *Clin. Dev. Immunol.*, vol. 2012, pp. 1–9, 2012, doi: 10.1155/2012/278059.
[66] T. E. Adolph *et al.*, "Paneth cells as a site of origin for intestinal inflammation," *Nature*, vol. 503, no. 7475, pp. 272–276, Nov. 2013, doi: 10.1038/nature12599.
[67] S. Bel *et al.*, "Paneth cells secrete lysozyme via secretory autophagy during bacterial infection of the intestine," *Science*, vol. 357, no. 6355, pp. 1047–1052, Sep. 2017, doi: 10.1126/science.aal4677.
[68] S. J. Gaudino *et al.*, "IL-22 receptor signaling in Paneth cells is critical for their maturation, microbiota colonization, Th17-related immune responses, and anti-Salmonella immunity," *Mucosal Immunol.*, vol. 14, no. 2, pp. 389–401, Mar. 2021, doi: 10.1038/s41385-020-00348-5.
[69] S. Ibiza *et al.*, "Glial-cell-derived neuroregulators control type 3 innate lymphoid cells and gut defence," *Nature*, vol. 535, no. 7612, pp. 440–443, Jul. 2016, doi: 10.1038/nature18644.
[70] A. B. Podany, J. Wright, R. Lamendella, D. I. Soybel, and S. L. Kelleher, "ZnT2-Mediated Zinc Import Into Paneth Cell Granules Is Necessary for Coordinated Secretion and Paneth Cell Function in Mice," *Cell. Mol. Gastroenterol. Hepatol.*, vol. 2, no. 3, pp. 369–383, May 2016, doi: 10.1016/j.jcmgh.2015.12.006.

[71] J. Wehkamp and E. F. Stange, “An Update Review on the Paneth Cell as Key to Ileal Crohn’s Disease,” *Front. Immunol.*, vol. 11, p. 646, 2020, doi: 10.3389/fimmu.2020.00646.
[72] W. M. De Vos, H. Tilg, M. Van Hul, and P. D. Cani, “Gut microbiome and health: mechanistic insights,” *Gut*, vol. 71, no. 5, pp. 1020–1032, May 2022, doi: 10.1136/gutjnl-2021-326789.
[73] A. M. Bolger, M. Lohse, and B. Usadel, “Trimmomatic: a flexible trimmer for Illumina sequence data,” Bioinformatics, vol. 30, no. 15, pp. 2114–2120, Aug. 2014, doi: 10.1093/bioinformatics/btu170.
[74] A. Dobin et al., “STAR: ultrafast universal RNA-seq aligner,” Bioinformatics, vol. 29, no. 1, pp. 15–21, Jan. 2013, doi: 10.1093/bioinformatics/bts635.
[75] Y. Liao, G. K. Smyth, and W. Shi, “featureCounts: an efficient general purpose program for assigning sequence reads to genomic features,” Bioinformatics, vol. 30, no. 7, pp. 923–930, Apr. 2014, doi: 10.1093/bioinformatics/btt656.
[76] M. I. Love, W. Huber, and S. Anders, “Moderated estimation of fold change and dispersion for RNA-seq data with DESeq2,” Genome Biol., vol. 15, no. 12, p. 550, Dec. 2014, doi: 10.1186/s13059-014-0550-8.
[77] Z. Fang, X. Liu, and G. Peltz, “GSEApy: a comprehensive package for performing gene set enrichment analysis in Python,” Bioinformatics, vol. 39, no. 1, p. btac757, Jan. 2023, doi: 10.1093/bioinformatics/btac757.
[78] N. Gicheva, M. S. Macauley, B. M. Arlian, J. C. Paulson, and N. Kawasaki, “Siglec-F is a novel intestinal M cell marker,” *Biochem. Biophys. Res. Commun.*, vol. 479, no. 1, pp. 1–4, Oct. 2016, doi: 10.1016/j.bbrc.2016.08.055.
[79] K. L. McDonald, “Out with the old and in with the new: rapid specimen preparation procedures for electron microscopy of sectioned biological material,” Protoplasma, vol. 251, no. 2, pp. 429–448, Mar. 2014, doi: 10.1007/s00709-013-0575-y.
[80] C. Rao, K. Z. Coyte, W. Bainter, R. S. Geha, C. R. Martin, and S. Rakoff-Nahoum, “Multi-kingdom ecological drivers of microbiota assembly in preterm infants,” Nature, vol. 591, no. 7851, pp. 633–638, Mar. 2021, doi: 10.1038/s41586-021-03241-8.
[81] M. A. McGuckin and D. J. Thornton, Eds., *Mucins: Methods and Protocols*, vol. 842. in Methods in Molecular Biology, vol. 842. Totowa, NJ: Humana Press, 2012. doi: 10.1007/978-1-61779-513-8.
[82] M. E. V. Johansson and G. C. Hansson, “Preservation of Mucus in Histological Sections, Immunostaining of Mucins in Fixed Tissue, and Localization of Bacteria with FISH,” in *Mucins*, vol. 842, M. A. McGuckin and D. J. Thornton, Eds., in Methods in Molecular Biology, vol. 842. , Totowa, NJ: Humana Press, 2012, pp. 229–235. doi: 10.1007/978-1-61779-513-8_13.

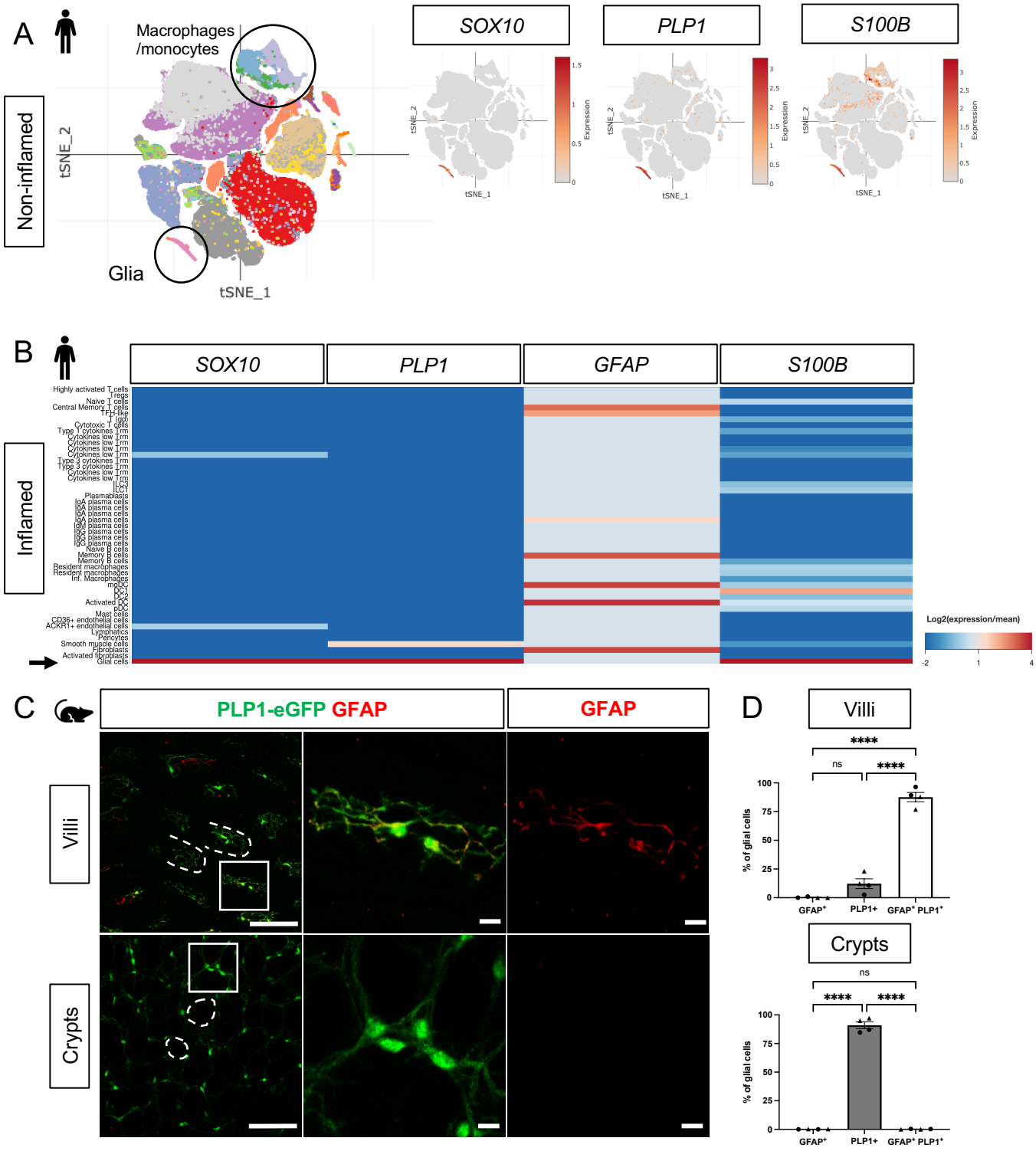

Figure 1. Mucosal glia in human and mouse small intestines widely express Plp1.

A) t-SNE plot of 94,451 cells isolated from terminal ileal mucosal biopsies from 13 children with non-inflammatory, functional gastrointestinal disorders [21], colored by annotated cell identity. *PLP1* and *SOX10* expression exhibits relative specificity to glia; the cells express high levels of these transcripts. *S100B* is expressed by glia as well as non-glial cells such as macrophages and monocytes. *GFAP* is undetectable in this dataset.

B) Heatmap of gene expression from 82,417 cells obtained by scRNAseq of mucosal biopsies from inflamed and non-inflamed segments of terminal ileum obtained from 11 adults with Crohn's disease [22]. In contrast to *PLP1*, *SOX10*, and *S100B*, which are most highly expressed in glia (arrow), *GFAP* expression is highest in non-glial cells.

C) Whole-mount immunostaining of ileum from an adult Plp1-eGFP mouse for GFAP imaged at the level of the villus- (top panels) and crypt-associated mucosa (bottom panels). Most glia in the villi express both PLP1 and GFAP while virtually all glia in the mucosa surrounding epithelial crypts are PLP1$^+$ and not immunoreactive for GFAP.

(D) Quantification of the percentages of GFAP$^+$, PLP1$^+$, GFAP$^+$PLP1$^+$ cells in the mucosa. Each data point represents an individual mouse, with triangles representing males and circles representing females. Scale bars = 100μm (large panels) and 20μm (magnified images). Error bars represent SEM. **** p<0.0001 by one-way ANOVA with Tukey multiple comparisons test.

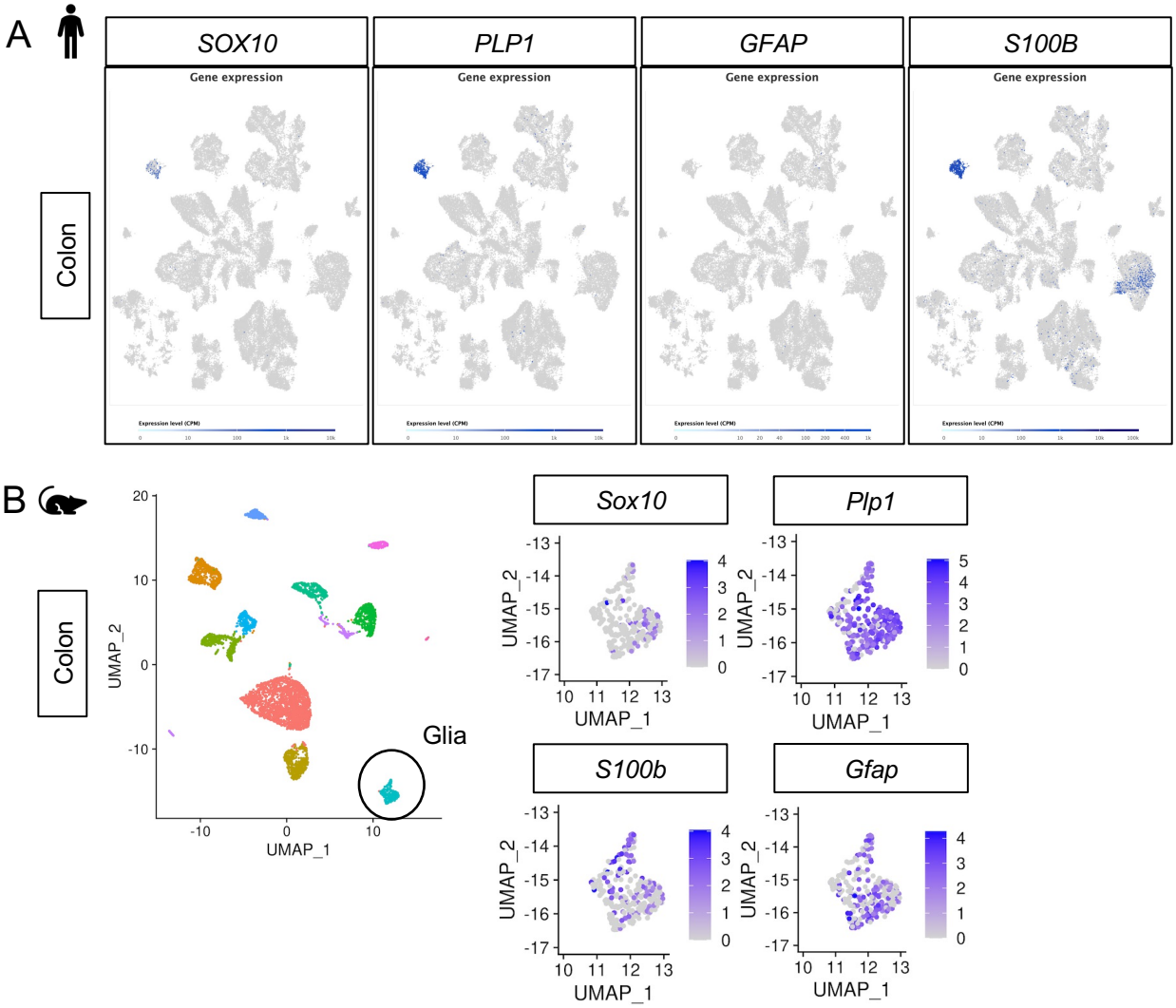

Supplementary Figure 1. Plp1 is the most specific and widely expressed marker of enteric glia in human and mouse colonic mucosa.

A) UMAP plots of 91,103 cells isolated from non-malignant colon tissues from 29 adult colorectal cancer patients [23]. *PLP1* marks most of the cells in the putative glial cluster while no *GFAP* is detected. *S100B* is robustly expressed by glia but also detectable in non-glial cells. *SOX10* is highly specific to the putative glial cluster but is not as universally detected within this cluster as *PLP1* and *S100B*.
B) UMAP plots of Drop-seq data from 3,179 mouse colonic mesenchymal/lamina propria cells [24]. *Plp1* is widely expressed in the putative glial cluster (301 cells) while *Sox10*, *S100b*, and *Gfap* exhibit narrower expression.

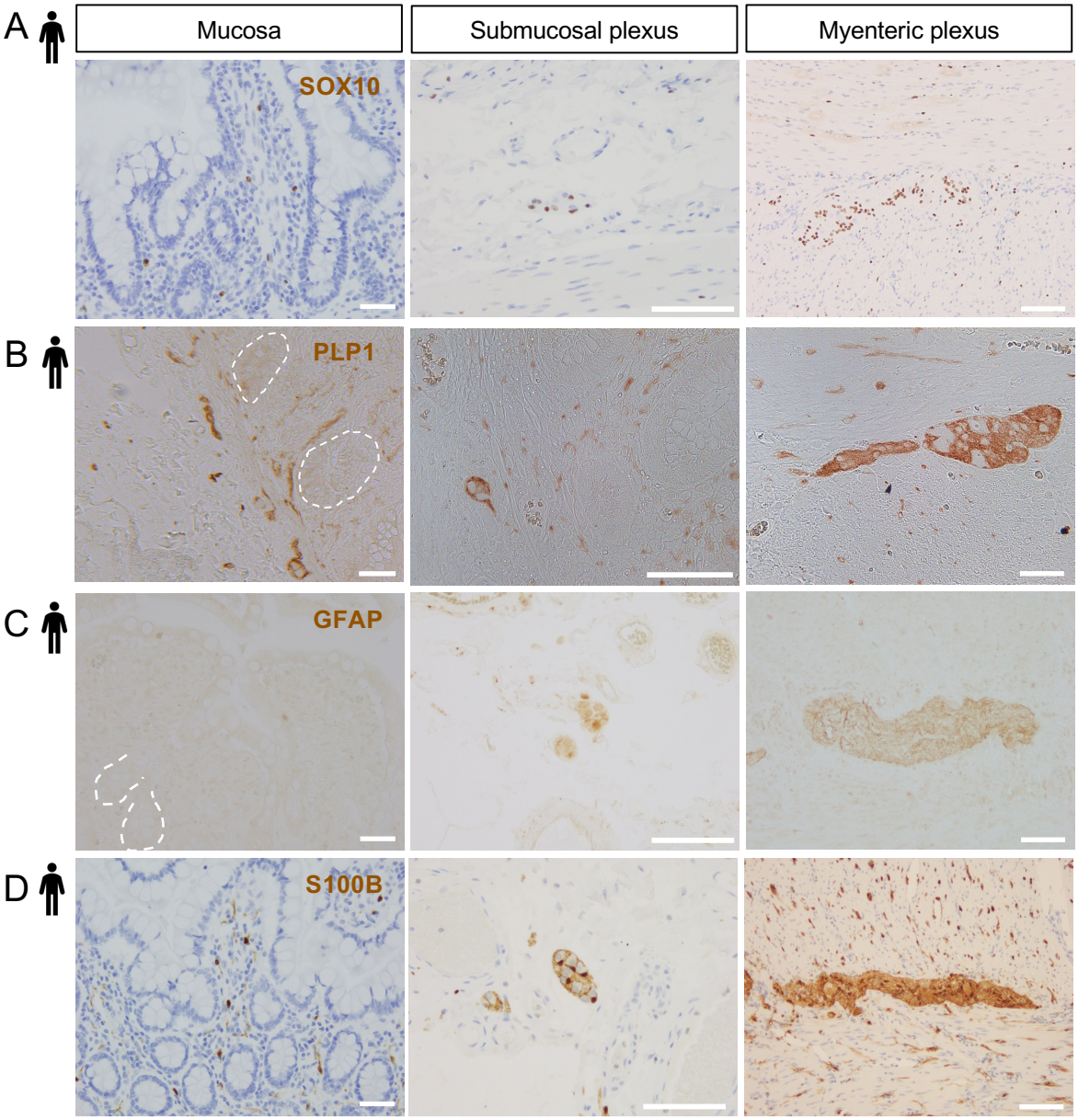

Supplementary Figure 2. S100B, SOX10, PLP1, and GFAP expression across the radial axis of the human small intestine.

A) – D) Representative IHC images of SOX10 (A), PLP1 (B), GFAP (C), and S100B (D) staining in non-diseased small intestinal tissue from adult females shown in three compartments: mucosa (left panels; selected crypts outlined in white for clarity), submucosal ganglia and the surrounding connective tissue and muscle (middle panels), and the myenteric plexus with surrounding circular and longitudinal muscle (right panels). SOX10, PLP1, and S100B were detected in all three compartments. GFAP immunoreactivity was detected in submucosal ganglia (middle panel) and myenteric ganglia (right panel), but not the mucosa. Images are representative of observations made in 5 of 5 subjects for SOX10 and S100B, 3 of 4 subjects for PLP1, and 3 of 3 subjects for GFAP. Scale bars = 100μm (left and right panels) and 50μm (middle panels).

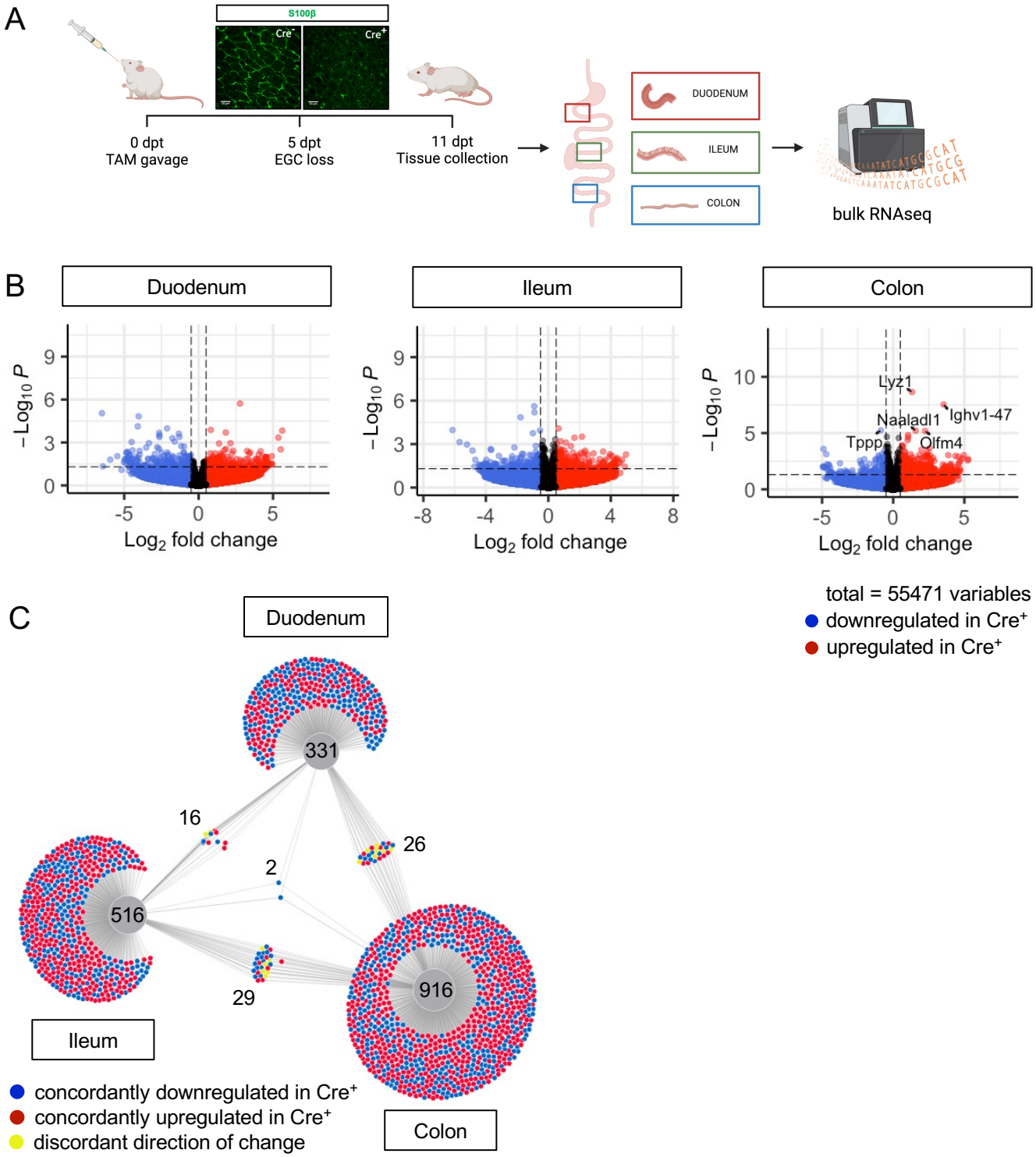

Figure 2. Glial ablation induces muted, region-specific transcriptional changes along the longitudinal axis of the intestine.

Figure 2. Glial ablation induces muted, region-specific transcriptional changes along the longitudinal axis of the intestine.

A) Schematic of the experimental timeline for bulk-sequencing of intestinal tissue segments from male $Plp1^{CreER}$ $Rosa26^{DTA/+}$ mice (annotated as Cre^{+}) and $Rosa26^{DTA/+}$ littermate controls (annotated as Cre^{-}). Tissues were collected 11 days after administration of tamoxifen (11dpt; n = 4 per genotype). In this model, the majority of enteric glial cells (EGC) are eliminated by 5dpt and the deficit is stable through at least 14dpt [12].
B) Volcano plots showing differentially expressed genes in duodenum, ileum, and colon of Cre^{-} and Cre^{+} mice. Genes that reached statistical significance cutoff of *padj* < 0.05 are labeled. Red and blue colors denote up- and down-regulated genes in Cre^{+} mice compared to Cre^{-} mice with p-value < 0.05, respectively. Differential analysis was conducted using DESeq2.
C) DiVenn analysis illustrates genes that were up- (red) or down-regulated (blue) in the duodenum, ileum, and colons of Cre^{+} mice compared to Cre^{-} controls at 11dpt with $p<0.05$ threshold for significance. Nodes linking tissues constitute the genes that were differentially expressed in Cre^{+} mice compared to controls in both of those tissues. Yellow color marks genes with discordant direction of change between the different tissue regions. Numbers indicate the number of genes at each node or tissue segment that were identified as differentially expressed. Overall, this analysis illustrates that most differentially expressed genes in Cre^{+} mice were region-specific with little overlap between duodenum, ileum, and colon.

A

Duodenum

Gene	pvalue	padj	log2FoldChange
Aldh3a1	0.000008910	0.1310646	-6.498995
Ighv1-58	0.000014900	0.1460164	-4.029232
Ly6g6c	0.000074400	0.5474189	-4.090178
Sprr1a	0.000103405	0.6086842	-2.120538
Igkv4-91	0.000212050	0.6934495	-2.653247
Nts	0.000239858	0.7059507	-1.333319
Ighv2-6-8	0.000313710	0.8393741	-2.630664
Igkv4-86	0.000399406	0.9400488	-1.288737
Saa3	0.000415216	0.9400488	-2.640961
Tcf23	0.000503807	0.9885368	-1.764401

Ileum

Gene	pvalue	padj	log2FoldChange
Hsd17b6	0.000002430	0.07120339	-0.9071903
Gstm3	0.000006480	0.09471883	-0.8888116
Igkv4-57	0.000014200	0.13850256	-1.7808468
Igkv4-62	0.000107928	0.55743722	-6.1350910
Tiparp	0.000114373	0.55743722	-0.5307053
Slc28a2b	0.000178179	0.74435683	-0.9921444
Nckap5	0.000591408	0.99998609	-0.3574527
Igkv12-38	0.000732130	0.99998609	-5.6854547
Ighv1-14	0.001072487	0.99998609	-5.2105739
Acpp	0.001167716	0.99998609	-0.4302563

Colon

Gene	pvalue	padj	log2FoldChange
Tppp	0.000005720	0.04042812	-0.8680251
Rasef	0.000021700	0.09222872	-0.4437229
Cxadr	0.000094800	0.26185200	-0.4071608
Omp	0.000162683	0.32591658	-0.4957502
Fchsd2	0.000174874	0.32591658	-0.3286969
Ssx2ip	0.000182448	0.32591658	-0.4090985
C730036E19Rik	0.000258691	0.40297592	-4.8994649
mt-Rnr2	0.000397022	0.54803483	-0.6238346
Ipmk	0.000485654	0.55662770	-0.4564745
Ralgds	0.000494894	0.55662770	-0.3194761

B

Duodenum

Gene	pvalue	padj	log2FoldChange
Ighv1-77	0.000001880	0.05546782	2.7875073
Jag2	0.000132530	0.62640252	0.8188377
Cited1	0.000148981	0.62640252	5.6165661
Igkv4-90	0.000202152	0.69344955	1.8245964
Gm42755	0.000458358	0.96360006	5.3594560
BC043934	0.001130218	0.99996906	2.1387513
Esrrb	0.001180178	0.99996906	1.3696598
Defa3	0.002827940	0.99996906	1.8367147
Gm38036	0.003046136	0.99996906	5.5153661
Ighv5-4	0.003383343	0.99996906	1.7316161

Ileum

Gene	pvalue	padj	log2FoldChange
Gm43697	0.000083600	0.5574372	0.6516949
Igkv5-39	0.000310037	0.9999861	2.1554750
Nr2f1	0.000365134	0.9999861	1.6719130
Fam189a2	0.000472555	0.9999861	0.4411970
Efna3	0.000636846	0.9999861	0.7792561
Doc2g	0.000790497	0.9999861	1.1183711
Rpgrip1l	0.000997760	0.9999861	0.5449431
Atp13a2	0.001101490	0.9999861	0.2951110
Gsdma2	0.001394452	0.9999861	1.4361176
Vmac	0.001425860	0.9999861	0.4085882

Colon

Gene	pvalue	padj	log2FoldChange
Lyz1	2.26000e-09	0.000068700	1.3220843
Ighv1-47	2.88000e-08	0.000437645	3.5427220
Naaladl1	6.16000e-06	0.040428115	1.5747556
Olfm4	6.66000e-06	0.040428115	2.2417255
Anpep	1.53000e-05	0.077245808	1.0413319
A530020G20Rik	2.43000e-05	0.092228715	1.0465385
Rbmx	2.74000e-05	0.092504400	0.3842134
Gm8437	4.28000e-05	0.129916521	1.0158035
Cirbp	1.18062e-04	0.298775154	0.6130367
4632404H12Rik	1.45657e-04	0.325916581	0.7008058

Supplementary Figure 3. Changes to whole tissue transcriptome resulting from glial ablation.

A - B) Top ten most down- (A, blue) and upregulated (B, red) genes in the duodenum, ileum, and colon of Cre^{+} mice compared to Cre^{-} mice, ordered by p-value. Differential gene expression analysis was performed using DESeq2.

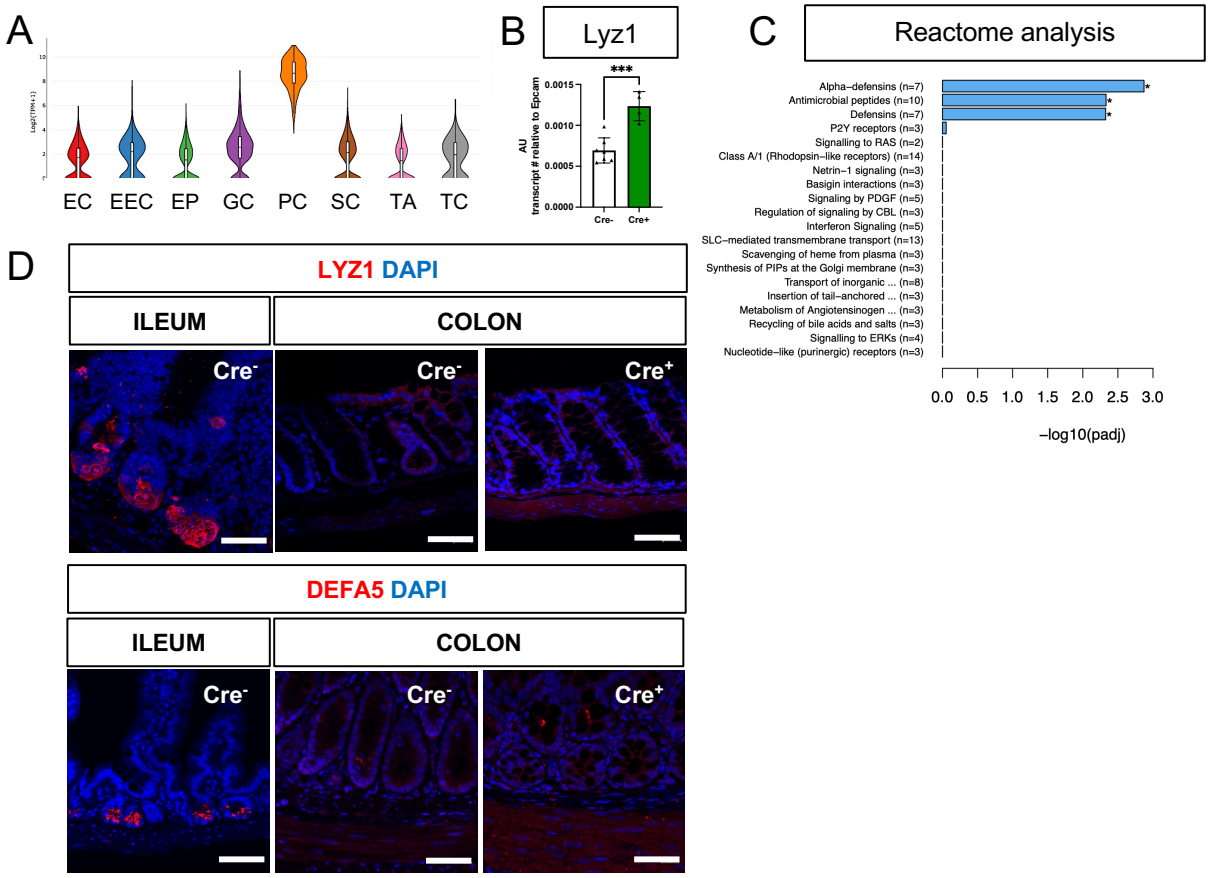

Supplementary Figure 4. Glial ablation induces colonic expression of *Lyz1* at the transcript, but not protein, level.

A) Violin plots of *Lyz1* expression in small intestine epithelial cells show enrichment of expression in Paneth cells (data from scRNAseq of mouse small intestine; [33]). EC – enterocyte, EEC – enteroendocrine cell, EP – enterocyte progenitor, GC – Goblet cell, PC – Paneth cell, SC – Stem cell, TA – Transient Amplifying cell, TC – Tuft cell.
B) Quantitative RT-PCR analysis of *Lyz1* expression in proximal colons of male Cre^- and Cre^+ mice. Each data point represents one mouse, with triangles representing males and circles representing females. Error bars represent SEM. ***$p<0.001$ by unpaired parametric *t*-test.
C) Reactome analysis of differentially expressed genes (significance threshold $p<0.05$) in colons of Cre^+ mice compared to Cre^- mice.
D) Representative IHC images of LYZ1 and DEFA5 staining in the distal ileums of Cre^- mice (positive control) compared to the proximal colons of Cre^+ and Cre^- mice (n=3 per genotype). No ectopic $LYZ1^+$ or $DEFA5^+$ cells were detected in the large intestines of glial-depleted mice. Scale bar = 50μm.

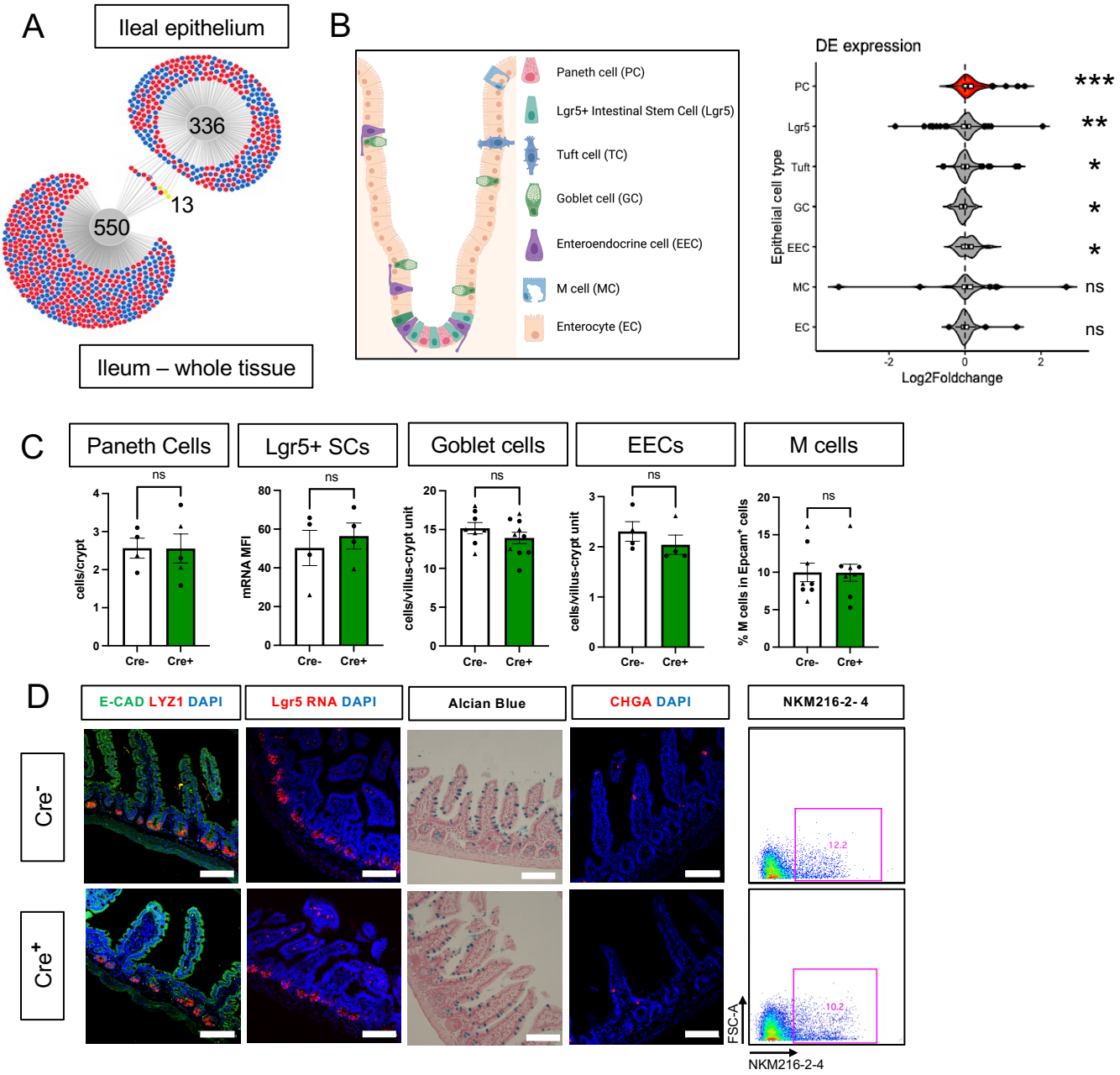

Figure 3. Glial ablation causes enrichment of specific epithelial cell type signatures without altering epithelial composition.

A) DiVenn analysis illustrates genes that were consistently up- (red) or down-regulated (blue) in the ileal epithelia and full-thickness ileal segments of Cre^+ mice compared to Cre^- controls at 11dpt with $p<0.05$ threshold for significance. Yellow color marks genes with discordant direction of change between the ileal epithelia and full-thickness ileal segments.
B) Schematic of various component cell types of the intestinal epithelium. Gene set enrichment analysis (GSEA) using single-cell gene signatures for epithelial cell types as defined in Haber *et al.*, 2017 ([33], Supplementary Table 1). The Paneth cell signature was most significantly enriched in the ileal epithelium of glia-depleted mice. Red color denotes the significant enrichment consistent across two independent GSEA. Thresholds for DE analysis: p-value <0.05. *** p<0.001, FDR <.001, ** p<0.001, FDR <0.01, * p<0.05, FDR <0.05, ns – non-significant.
C - D) Quantification of epithelial subtypes in the small intestines of Cre^- and Cre^+ mice with representative IHC images and flow cytometry plots below each graph showing the marker and approach used for cell identification. Each data point represents an individual mouse, with triangles representing males and circles representing females. Error bars represent SEM. ns - not significant by unpaired parametric *t*-test. Scale bar = 100μm. E-Cadherin (E-CAD) labels cell borders, LYZ1 marks Paneth cells, *Lgr5* transcript expression marks intestinal stem cells (SCs), Alcian blue marks goblet cells, Chromogranin A (CHGA) marks enteroendocrine cells, and NKM216-2-4 identifies microfold (M) cells by flow cytometry. Cell nuclei are labeled with DAPI (blue) in the IHC panels.

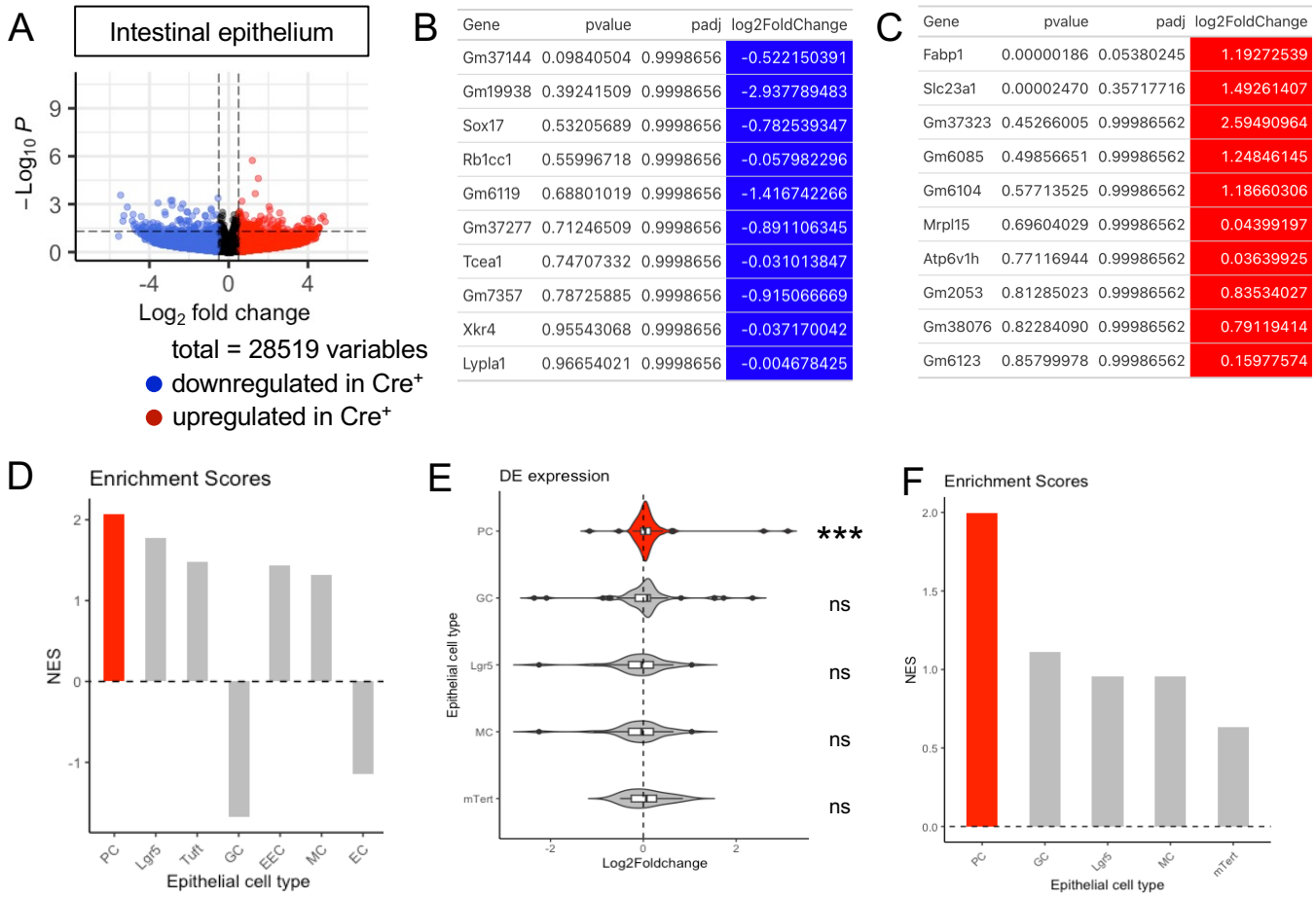

Gene	pvalue	padj	log2FoldChange
Gm37144	0.09840504	0.9998656	-0.522150391
Gm19938	0.39241509	0.9998656	-2.937789483
Sox17	0.53205689	0.9998656	-0.782539347
Rb1cc1	0.55996718	0.9998656	-0.057982296
Gm6119	0.68801019	0.9998656	-1.416742266
Gm37277	0.71246509	0.9998656	-0.891106345
Tcea1	0.74707332	0.9998656	-0.031013847
Gm7357	0.78725885	0.9998656	-0.915066669
Xkr4	0.95543068	0.9998656	-0.037170042
Lypla1	0.96654021	0.9998656	-0.004678425

Gene	pvalue	padj	log2FoldChange
Fabp1	0.00000186	0.05380245	1.19272539
Slc23a1	0.00002470	0.35717716	1.49261407
Gm37323	0.45266005	0.99986562	2.59490964
Gm6085	0.49856651	0.99986562	1.24846145
Gm6104	0.57713525	0.99986562	1.18660306
Mrpl15	0.69604029	0.99986562	0.04399197
Atp6v1h	0.77116944	0.99986562	0.03639925
Gm2053	0.81285023	0.99986562	0.83534027
Gm38076	0.82284090	0.99986562	0.79119414
Gm6123	0.85799978	0.99986562	0.15977574

Supplementary Figure 5. Transcriptional profiling of the ileal epithelium in glial-ablated mice reveals enrichment of Paneth cell signatures.

A) Volcano plots showing differentially expressed genes in ileal epithelia of Cre$^-$ and Cre$^+$ mice. Red and blue colors denote up- and down-regulated genes in Cre$^+$ mice compared to Cre$^-$ mice with p-value < 0.05, respectively. No genes reached statistical significance cutoff of *padj* < 0.05. Differential analysis was conducted using DESeq2.
B and C) ÅTop ten down- (B) and upregulated (C) genes in the ileal epithelia of Cre$^+$ mice compared to Cre$^-$ controls, ordered by p-value. Differential analysis was conducted using DESeq2.
D) Related to Main Figure 3B. Normalized enrichment scores from GSEA performed using cell-type specific signatures derived from scRNAseq study of the ileal epithelium ([33], Supplementary Table 1). Red color denotes the significant enrichment consistent across two independent GSEA.
(E) Log2fold change from GSEA of epithelial cell type-specific gene signatures in Cre$^+$ vs. Cre$^-$ ileal epithelium using cell signatures curated from studies that used transcriptional profiling of individual cell types purified by genetic reporter expression (see Supplementary Table 2 for gene lists). This identifies the Paneth cell signature as most enriched in glial-depleted mice. Thresholds for DE analysis: p-value <0.05. *** p<0.001, FDR<0.001.
(F) Related to (E), normalized enrichment scores from GSEA.

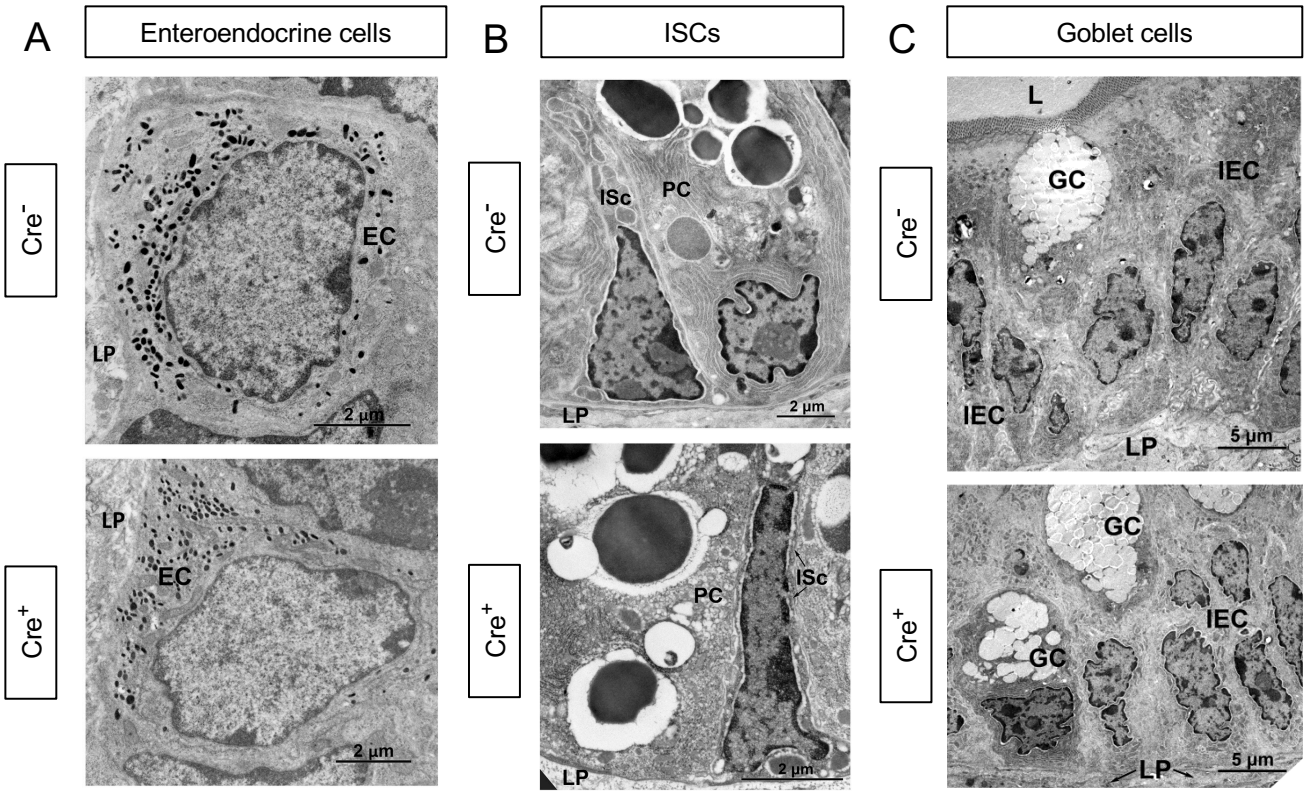

Supplementary Figure 6. Glial depletion does not affect the ultrastructure of enteroendocrine, crypt base stem cells, or goblet cells.

A - C) Transmission electron microscopy of enteroendocrine cells (A; EC), crypt base intestinal stem cells (B; ISc), and goblet cells (C; GC) reveal no changes in the morphology of these cells in 9dpt Cre^+ mice compared to Cre^- littermate controls studied in parallel. Representative images are from n = 2 mice per genotype from independent cohorts. IEC, Intestinal Epithelial Cell; LP, Lamina propria; L, Lumen; PC, Paneth cell. Scale bar = (A-B) 2µm, (C) 5µm.

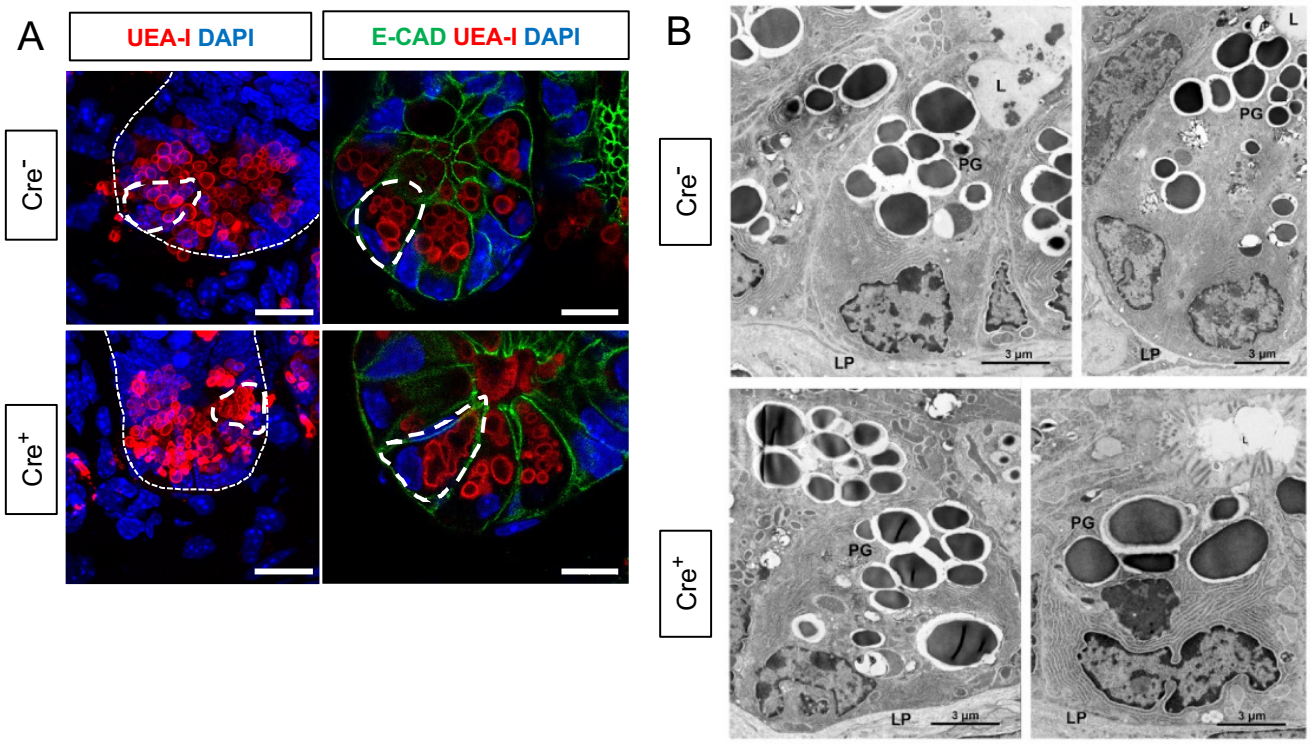

Figure 4. Glial depletion triggers morphological changes in Paneth cells.

A) Representative images of UEA-I staining of Paneth cell granules in the small intestine of Cre^- and Cre^+ mice (observed in at least 3 mice per genotype). Scale bar = 10µm.
B) Representative transmission electron microscopy images of Paneth cells (n = 2 mice per genotype from independent cohorts). Paneth cells in Cre^+ mice are globular, exhibit loss of polarity, and have heterogeneous granules (PG). L, Lumen of the intestinal crypts; LP, lamina propria. Scale bar = 3µm.

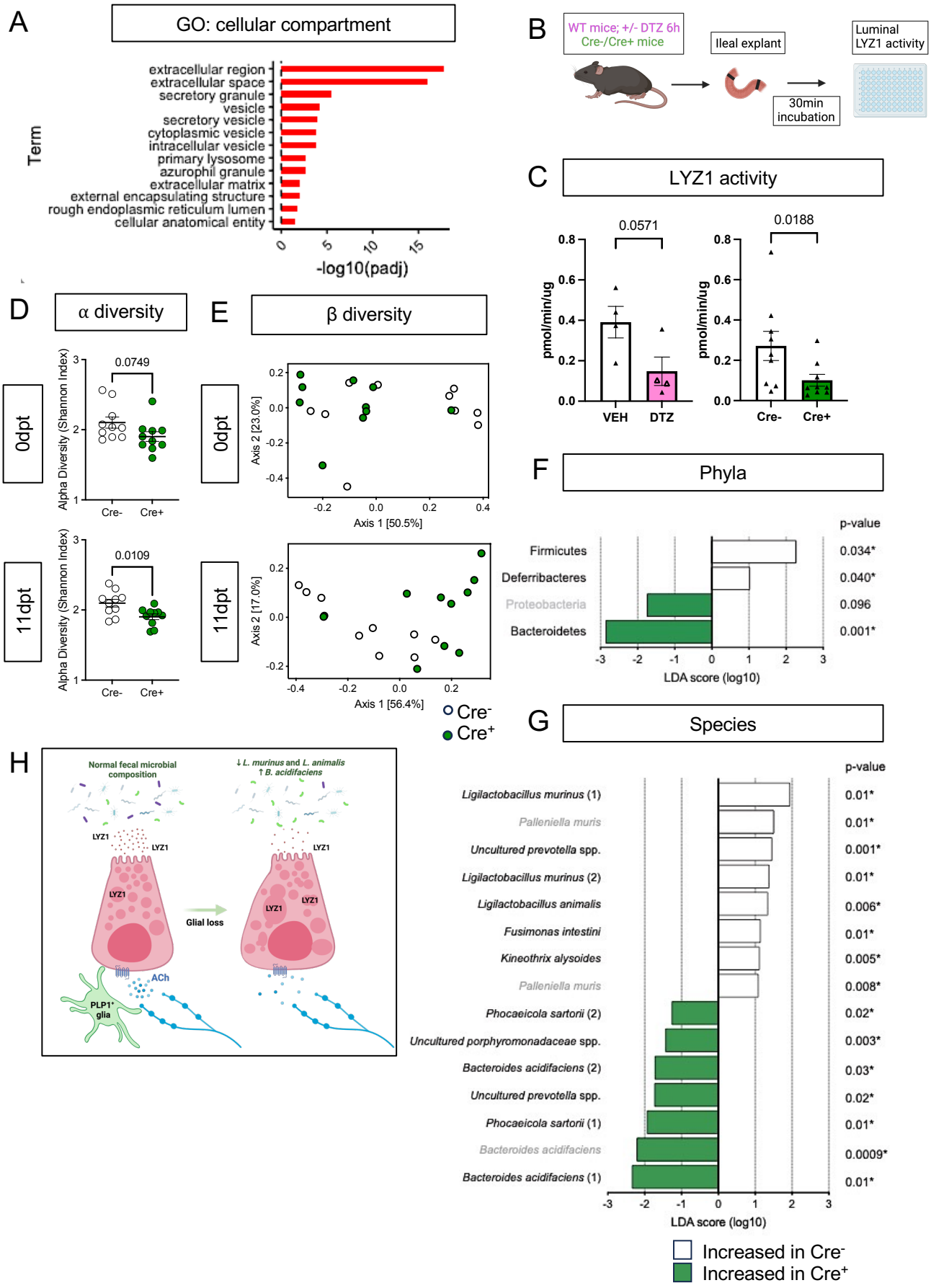

Figure 5. Enteric glial depletion impairs Paneth cell secretion and alters the composition of the gut microbiome.

Figure 5. Enteric glial depletion impairs Paneth cell secretion and alters the composition of the gut microbiome.

A) Pathway analysis using GO term for cellular compartment shows significant enrichment of Paneth cell genes in glial-depleted mice.
B) Schematic of explant assay used to analyze Paneth cell secretion. Small intestinal explants were acutely isolated, ligated at both ends, and incubated in oxygenated media at 37^{o}C for 30min. Luminal contents were then extracted and analyzed for lysozyme activity by fluorometric assay.
C) Luminal lysozyme activity was lower in ileal explants from Cre^{+} mice compared to Cre^{-} controls (p=0.0188), mirroring the effects of Paneth cell disruption by dithizone (DTZ) in wildtype mice (p=0.0571). Each data point represents one mouse (n = 4 per treatment, n= 9 mice per genotype). Open triangles in DTZ group represent subset of explants incubated with 10μM carbachol to stimulate secretion. Error bars represent SEM. ns – non-significant, p values shown are from Mann-Whitney U test.
D – G) Microbiome analysis by 16S rDNA sequencing of fecal pellets from Cre^{-} and Cre^{+} mice at 0dpt (baseline, pre-induction) and 11dpt. Graphs depict α-diversity (D) and β-diversity (E) with each data point representing one mouse. Error bars represent SEM. p-values reflect unpaired parametric *t*-test. Analysis of phylum- (F) and species- (G) specific differences at 11dpt using LEfSe ($p<0.1$, LDA>1, FDR-adjusted significance values provided). Any phyla or species detected as differentially abundant at baseline are demarcated in grey.
H) Working model of glial regulation of Paneth cell function. In the normal intestine, Paneth cells are loaded with secretory granules containing LYZ1 that are released into the gut lumen in response to acetylcholine (Ach) and other signals to regulate microbial composition. Upon glial depletion, Paneth cell secretion is disrupted leading to dysmorphic granules, diminished LYZ1 secretion, and altered fecal microbial composition. This occurs without a change in Paneth cell number, loss of muscarinic acetylcholine receptor expression, or denervation of the cholinergic fibers that normally surround epithelial crypts.

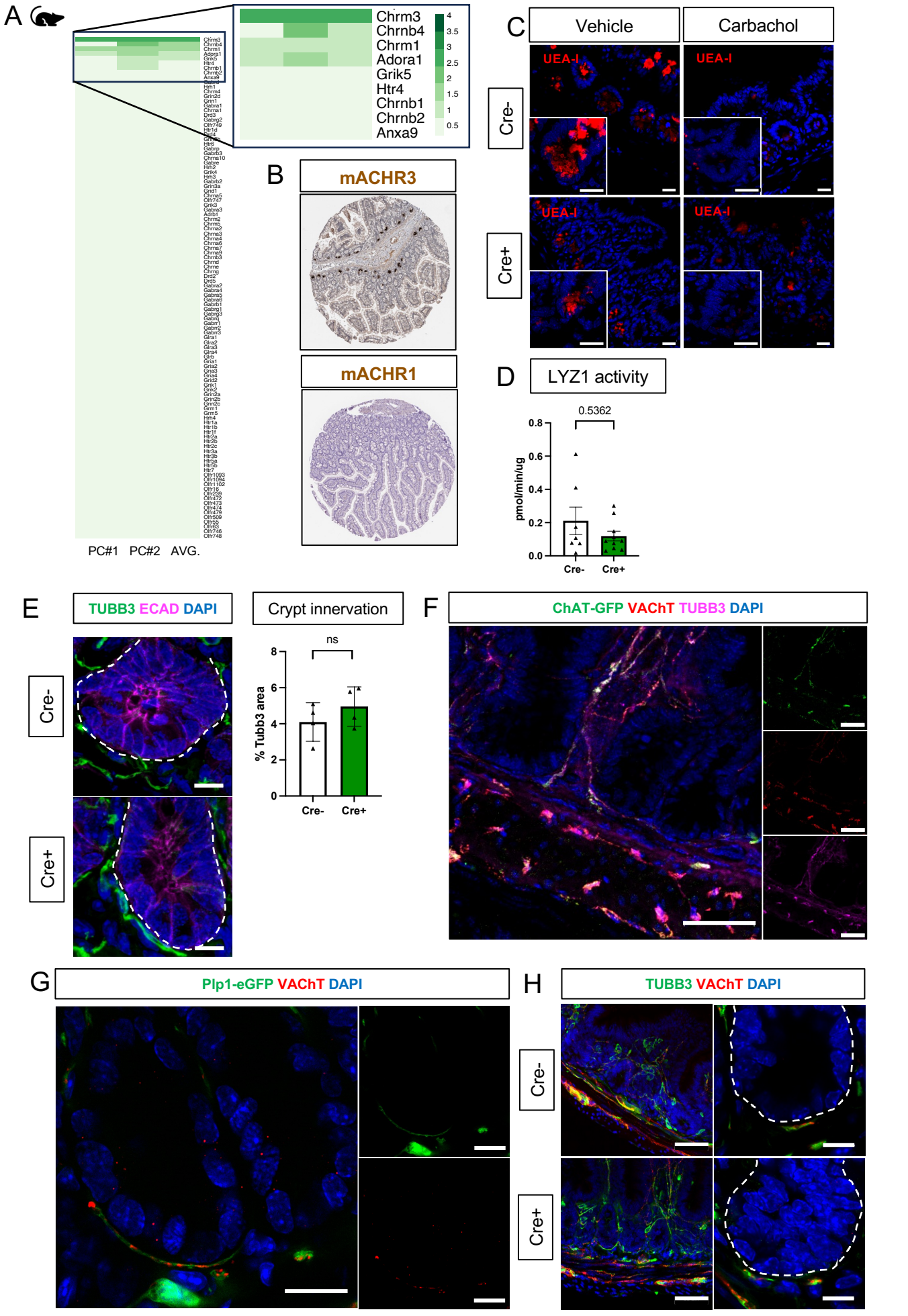

Supplementary Figure 7

Supplementary Figure 7. Depletion of enteric glia does not alter epithelial crypt innervation.

A) Heatmap of neurotransmitter receptor gene expression following GSEA of publicly available RNAseq data from mouse Paneth cells isolated by cell sorting [52] using an Qiagen Ingenuity Pathway Analysis gene set for neurotransmitter receptors. A subset of genes encoding receptors for acetylcholine, specifically Chrm3, Chrnb4, and Chrm1, exhibit the strongest expression in Paneth cells.
B) Representative images of immunohistochemistry for mAChR3 (n=2) and mAChR1 (n=1) in the human small intestine show high expression of mAChR3 (encoded by *CHRM3*) in Paneth cells (Protein Atlas, www.proteinatlas.org).
C) Representative images of cross-sections of ileum from explants isolated from Cre^- and Cre^+ mice, incubated with the cholinergic agonist carbachol (10μM) or vehicle for 30min, and stained with UEA-I (red) to label Paneth cell granules (n=3 mice per condition). Paneth cells in both groups of mice showed robust degranulation of UEA-I^+ granules upon cholinergic stimulation. Scale bar = 20μm.
D) Lysozyme activity in luminal contents of ileal explants from Cre^- and Cre^+ mice following incubation with carbachol (10μM) for 30min. No difference between explants from Cre^- and Cre^+ mice was detected. Each data point represents one mouse (n = 7-10 mice per genotype). Error bars represent SEM. ns – no significant difference in means by Mann-Whitney U test.
E) Representative images of intestinal epithelial crypts from ileal segments of Cre^- and Cre^+ mice immunostained for ECAD (magenta) to label epithelial cell borders and TUBB3 (green) to label nerve fibers. Individual crypt outlined by a dashed line. Quantification of crypt-proximal $TUBB3^+$ neuronal fibers reveals no difference between Cre^- and Cre^+ mice (n = 4 mice per genotype). Error bars represent SEM. ns - no significant difference in means by unpaired parametric *t*-test. Scale bar = 10μm.
F) IHC for VAChT (red) and TUBB3 (magenta) in the ileum of an adult ChAT-GFP mouse. The majority of TUBB3 immunoreactivity around epithelial crypts colocalizes with GFP (green), indicating that cholinergic fibers (green) comprise most of the crypt-innervating fibers. Scale bar = 50μm.
G) IHC for VAChT (red) to label cholinergic fibers in the ileum of an adult PLP1-eGFP mouse in which Plp1-expressing enteric glia are labeled with GFP (green). GFP^+ glia are tightly associated with crypt-innervating cholinergic fibers. Scale bar = 10μm.
H) IHC for TUBB3 (green) and VAChT (red) in the ileums of Cre^- and Cre^+ mice. Individual crypts are magnified in the right panels and outlined by dashed lines. Crypt innervation by fibers labeled with either marker was no different between control and glial-ablated mice. Scale bar = 50μm (left panels) and 10μm (right panels).
Images in F-H are representative of observations made in 3 mice per genotype.

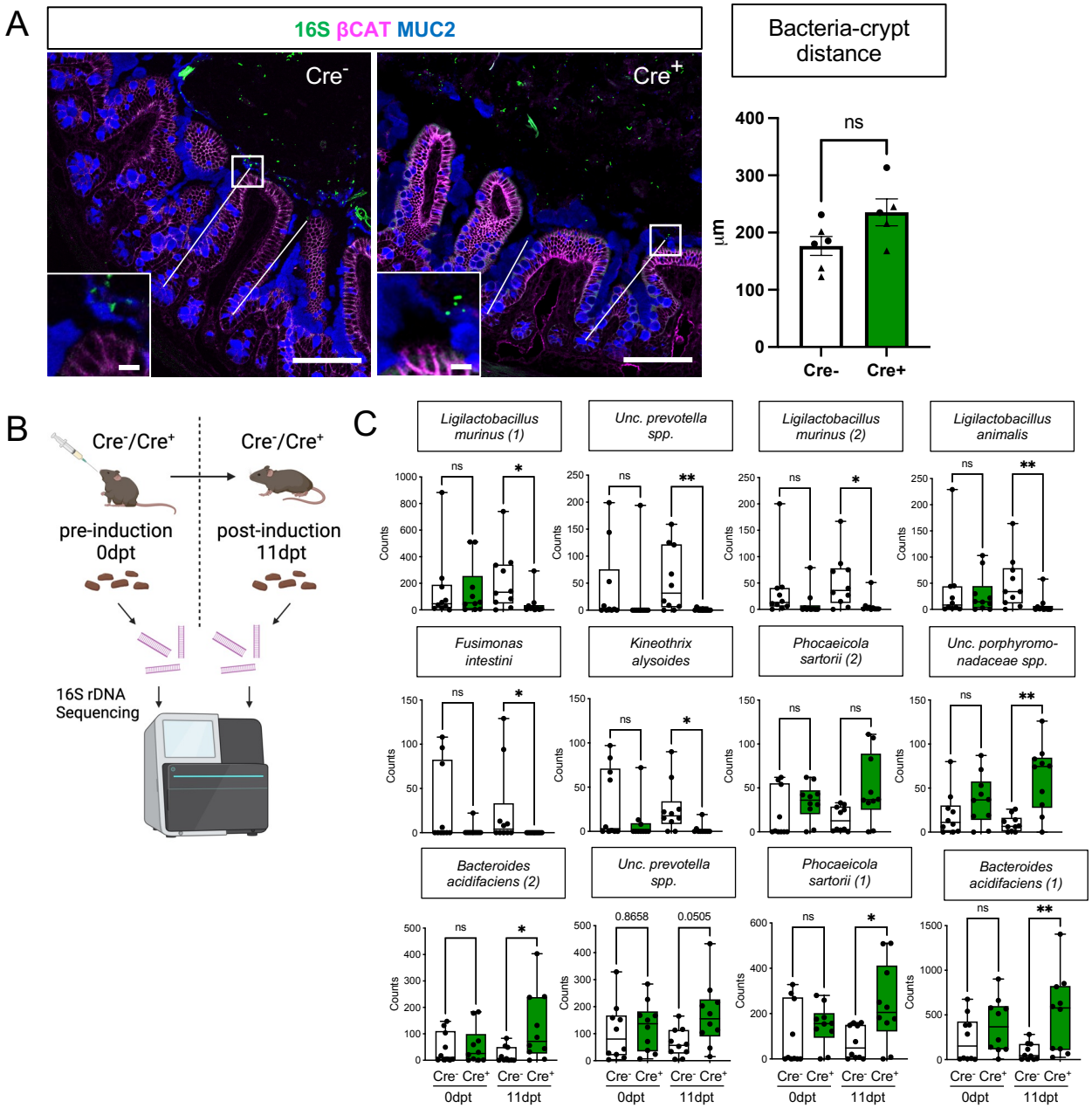

Supplementary Figure 8. Glial depletion alters gut microbial composition but not the spatial relationship between the host and the bacteria. Related to Figure 5.

A) Representative images of 16S rRNA bacterial fluorescent in situ hybridization (green) with IHC for MUC2 (blue) and beta-catenin (magenta) in Cre$^+$ and Cre$^-$ mice to visualize bacteria, mucus, and epithelial cell borders, respectively. The distance of the closest bacterial signal to the center of >50 open crypts/mouse was measured and average values per mouse are shown in the graph. Each data point represents one mouse, with triangles representing males and circles representing females. Error bars represent SEM. ns– non-significant by unpaired t-test. Scale bar = 100µm (large panels) and 10µm (insets).

B) Schematic of experimental design for microbiome analysis. Fecal pellets from Cre$^-$ and Cre$^+$ mice pre- (0dpt) and post- (11dpt) induction were analyzed with 16S rDNA sequencing.

C) Four-way analysis of species identified as differentially abundant between Cre$^-$ and Cre$^+$ mice at 11dpt but not 0dpt (related to Main Fig. 5G). Each data point represents one mouse; both males and females were used. *p<0.05; **p<0.01; ns – non-significant by Dunn's multiple comparison test, following Kruskal-Wallis test.